Physics, Chemistry and Engineering Sciences
Functional Materials and their Technological Applications

Contents

Frontiers in Science and Engineering
International Journal

Physics, Chemistry and Engineering Sciences
Functional Materials and their Technological Applications

Contents

WELCOME TO FSE

Frontiers in Science and Engineering, an International Journal edited by The Hassan II Academy of Science and Technology uses author-supplied PDFs for all online and print publication.

The objective of this electronic journal is to provide a platform of exchange of high quality research papers in science and engineering. Though it is rather of wide and broad spectrum, it is organized in a transparent and simple interactive manner so that readers can focus on their direct interest.

All papers are submitted to the normal peer-review process. Publication criteria are based on :
i) Novelty of the problem or methodology and problem solving, **ii**) Salience of the approach and solution technique, **iii**) Technical correctness and outputs, **iv**) Clarity and organization.

Papers are first reviewed by the Executive Board Director who receives the paper and, if relevant in terms of the overall requirements, it is then proposed to one of the most appropriate associate editor on the field who will select 2 to 3 expert reviewers. Electronic printing will allow considerable time savings for submission delays which will be reduced drastically to less than three to six months. Prospective authors are therefore invited to submit their contribution for assessment while subjected to similar quality criteria review used in paper journals.

Authors are notified of acceptance, need for revision or rejection of the paper. It may be noted that papers once rejected cannot be resubmitted. All the details concerning the submission process are described in another section. This electronic journal is intended to provide :

- the announcement of significant new results,
- the state of the art or review articles for the development of science and technology,
- the publication of proceedings of the Academy or scientific events sponsored by the Academy,
- the publication of special thematic issues.

So that the scientific community can :
- promptly report their work to the scientific community,
- contribute to knowledge sharing and dissemination of new results.

The journal covers the established disciplines, interdisciplinary and emerging ones. Articles should be a contribution to fundamental and applied aspects, or original notes indicating a significant discovery or a significant result.

The topics of this multidisciplinary journal covers amongst others :
Materials Science, Mathematics, Physics, Chemistry, Computer sciences, Energy, Earth Science, Biology, Biotechnology, Life Sciences, Medical Science, Agriculture, Geosciences, Environment, Water, Engineering and Complex Systems, Science education, Strategic and economic studies, and all related modeling, simulation and optimization issues, etc. ...

Once, a certain number of papers in a specific thematic, is reached, the Academy might edit a special paper issue in parallel to the electronic version.

PRESENTATION NOTE

Frontiers in Science and Engineering is an International Journal published by Hassan II Academy of science and Technology. In its nature, it is a multidisciplinary scientific journal and follows the rule of Frascatti international science classification of scientific areas.

Our Online Publications System Manager is an electronic publications system of an open access journal providing trimester/semester/annual publications of papers in all areas of the major aspects.

However as this covers a wide spectrum, we will restrict ourselves to 5 major areas:
- **Mathematics, Computer Science and Computational Applications (GRIS**
- **Physics, Chemistry and Engineering Sciences**
- **Life Sciences (Medical, Health, Agriculture, Biology, Genetics)**
- **Earth Sciences (Earth, Water and Oceans, Environmental Sciences)**
- **Strategic Studies and Economic Development**

All papers are subjected to peer-review by members of an editorial board or qualified reviewers and if accepted will be published in less than two months time.

The multi-journal welcomes the submission of manuscripts that meet the general scope and criteria's as described in our website.

The authors will be noticed the decision of manuscripts within 4 weeks after submission. Accepted articles will normally be published during the next 4 weeks.

Publication Fee: free

For more and detailed information please visit : http://www.academie.hassan2.sciences.ma/fse/

Frontiers in Science and Engineering - Vol. 5 - n°2 - 2015
An International Journal Edited by The Hassan II Academy of Science and Technology

II

FOREWORD

This special issue of Frontiers in Science and Engineering (FSE) contains selected papers presented at the International Conference on "Functional Materials and their Technological Applications" held at Ecole Normale Supérieure (ENS) of Casablanca- Hassan II university of Casablanca, 24-25 October 2014. The aim of this conference is to provide participants the opportunity to present the new progress of their work and to make a development of the state of the art of the field of functional materials. A particular attention to the application of these functional materials in new technologies was stressed. The main conference objectives are to:

- Promote research in the field of advanced materials with respect to nature;
- Deepen the knowledge of young researchers;
- Strenghten national and international exchange;
- Address various topics in a multidisciplinary way to highlight the various applications and fields of cooperation.

Furthermore, papers in several research areas are presented in this special issue. For the sake of illustration: renewable energy with modeling and simulation of the incident solar radiation on a horizontal and an inclined plane, detailed theoretical and numerical studies for PV characterization, study the crack diffusion created at single region of composite materials by using the fiber bundle model, study of different growth mechanisms and morphology of Al-thin film on Ni(100) substrate at 300 K, using molecular dynamics simulation, a new method for preparing silver nanofluids based on self assembly process, a mathematical model to determine the crack depth from the standard thermal contrast taking into account the contrast time values.

The organisers were fortunate to welcome outstanding scientists in the fields of optical material, optoelectronics, materials sciences and technology including the plenary speakers, i.e. Prof. Murielle Eyraud, University of Marseille (France), Prof. Bouchta Sahraoui, University of Angers (France), Prof. Mohammed Rguiti, University of Valenciennes (France) and Jean Ebothé of Reims University (France).

We wish to thank various institutions, and associations, which provided support for the conference, and more particularly to ENS of Casablanca, Hassan II university of Casablanca and the Moroccan Association of Physics of Advanced Materials and their Applications (SMPM2A). We would like also to acknowledge the sponsorship of Hassan II Academy of Science and Technology, and for accepting to devote this special issue of Frontiers in Science and Engineering to "Functional Materials and their Technological Applications".

Guest Editor
Prof. Yahia BOUGHALEB
Chouaib Doukkali University.

For FSE
Prof. Driss Ouazar
Resident Member of Hassan II Academy of Science and Technology (Executive Director).

Study of crack diffusion in composite materials using the fiber bundle model

I. Achik[a], A. Hader[a,b], H. Sbiaai[a] , Y. Boughaleb[a, c,*]

[a] Ecole Normale Supérieure, Université Hassan II de Casablanca, Morocco

[b] Centre régional des métiers d'éducation et de formation Settat, Morocco

[c] Université Chouaib Doukkali, EL Jadida, Morocco

Abstract. Our aim is to investigate the crack diffusion created at single region of composite materials by using the fiber bundle model. So, we have applied an external single crack in one fiber of the composite material, and we then continue to increase this load at a very slow rate until the considered fiber breaks and its load is redistributed to its neighboring intact ones. This breaking and redistribution dynamics repeat itself and this process ensures an advancing interfacial fracture and the area of the damaged region increases with time until a final crack of material. Our calculations are done in the context of the local load-sharing rule. The results show that the damaged region area increases with time by following the Lifshitz-Slyozof law with an exponent growth x=2. This permits us to deduce the behavior of the crack diffusion with the applied load. The corresponding results of the life time materials exhibit an exponential decreasing with the applied load and a linear decreasing with temperature.

PACS numbers: 62.20.Mk; 62.20.Hg; 81.05.-t; 61.43.-j

Keywords : *the crack correlation function*; Fiber bundle model; the crack diffusion coefficient, Thermal noise.

I. Introduction

Focusing on the use of naturally different substances in the onset frucster has ever been the issue of several surveys in the engineering community for its mere technological developments. In fact, the somatogenetic handling, sometimes meant as an indispensable separation, is apparently causing a vast waste of time for extreme macroscopic blockage of the solid, while depending on the amplitude of the applied stress[1–3]. That is why scientists are actually devoting a great deal of time to tackle many theories and experiments for the clarification of the unpredictable fractures, e.g., the velocity of propagation, the roughness, and the onset of precursors.

In the contrast, the fiber bundle model describes a collection of elastic fibers under load. The fibers fail successively and for each failure, the load distribution among the surviving fibers changes. Even though very simple, this model captures the essentials of failure processes in a large number of materials and settings. This model has been studied extensively since it can be analyzed to an extent that is not possible for more complex materials [4–6]. The statistical distribution of the magnitude of avalanche phenomenon in fiber bundles is well studied [7–9], and the failure dynamics under constant load has been investigated through recursion relations which in appears a phase transitions and associated critical behavior in this

---

* Corresponding author: ahader73@yahoo.fr

Frontiers in Science and Engineering - Vol. 5 - n°2 - 2015
An International Journal Edited by The Hassan II Academy of Science and Technology

1

model [10]. However, there are two extreme rules which consider a bunch of fibers hanging from a rigid ceiling and a platform is connected to the ends of these fibers and a load hangs from that plat form. Once the fibers begin to fail, we can distinguish two transfer load type: Global load sharing (GLS) in which the load of a broken fiber is equally shared with all intact fibers in the whole system. We assume a long-range interaction among the fibers and we treat analytically the problem by using the mean-field approximation [3]. The other type consist in a local load sharing (LLS), in which the terminal load of the failed fiber is distributed equally to all the nearest neighboring intact fibers.

Hence, one creates the initial applied load localized at an arbitrarily chosen central site in the frame work of the local load-sharing fiber bundle model. So, initially, no load is applied on any fiber except for the one at the central site. As the applied load increases beyond the failure threshold of this central fiber, it breaks and the load carried by it is redistributed among its nearest neighbors and so on.

In this paper, we study the crack diffusion in composite materials subject to a local load-sharing fiber bundle model in two dimensions under an external load applied at a single point. By the use of the local load-sharing rule, the redistributed load remains localized along the boundary of the broken patch.

II. THE MODEL

The fiber pack product identifies accumulation flexible materials below load. Under some conditions when the length of the fibers of the composite material exceeds its breaking critical value, the material cracks [11]. So, for every single disappointment, the strain circulation one of the remaining materials changes. Ergo, that creates a feedback method that could make the sum total disappointment of the system. Although quite simple, that product reflects the necessities of disappointment procedures in a significant number of components and settings. We provide here evaluation the fiber pack product with various fill redistribution elements from the function of see of data and mathematical science as opposed to components technology, with an emphasis on ideas such as for example criticality, universality and fluctuations.

We contemplate a deal of size *M* consisting of a big quantity of materials held at equally ends. We examine equal-load-sharing versions in which the fill formerly moved by an unsuccessful fiber is distributed similarly by closest friend unchanged materials [12–15]. The pack middle is at the mercy of an area regular additional tension similar to the fibers direction. The strain moved by that fiber is redistributed similarly among their closest remaining neighbor(s). In that way, the materials which are just confronted with the strain, state, following an avalanche, has a somewhat minimal fill than the people that are accumulating fill gives from the sooner problems and surviving. Within our function we think that the original regional load f_0 is likely to be corresponding to the unchanged materials which stimulate an original elongation δl_0 distributed by the Hooke›s legislation:

$$\delta l_0 = f_0 / k \qquad (1)$$

where *k* denotes the stiffness, which is assumed to be the same for all the fibers. The local elongation of fibers *i* have time-dependent fluctuations due to the presence of thermal noise load and to load transfer following breaking events given by:

$$\xi_i = \gamma l_0 \sqrt{K_B T} \qquad (2)$$

where l_0 is the initial length of fibers and K_B is the Boltzmann constant and is coefficient of proportionality. The presence of the thermal noise will affect the lifetime for a constant applied stress controlled by the temperature *T* of the system [2,9].

So, the actual stress arising δl_i of fiber *i* is written as:

$$\delta l_i = \delta l_0 + \xi_i \qquad (3)$$

III. THE RESULTS

Originally we used a lot on a single fiber devoted to the material. We then keep on to boost force at a really gradual charge before the focused fiber pauses; force moved by its redistributed similarly among their four neighbors. Because we keep on to boost force just on the materials which are presently holding a nonzero fill, that breaking and redistribution character replicate itself. This method guarantees a developing interfacial fracture and the location of the ruined location raises. That subject has been commonly learned around years, equally theoretically and experimentally [16-17] in the Plexiglas try out two dishes were taken and condition was presented by sandblasting and then were joined together creating a clear stop by having a simple plane. Therefore, when we continue to increase the external load, the material cracks totally at time t_f. So, the corresponding results of the calculation of the lifetime are plotted in fig 1. We remark clearly that the lifetime decreases exponentially with the applied load. The same result has been found in the two cases when we applied the external load on all intact fibers of the materials (LLS rule [2] and GLS rule [3]).
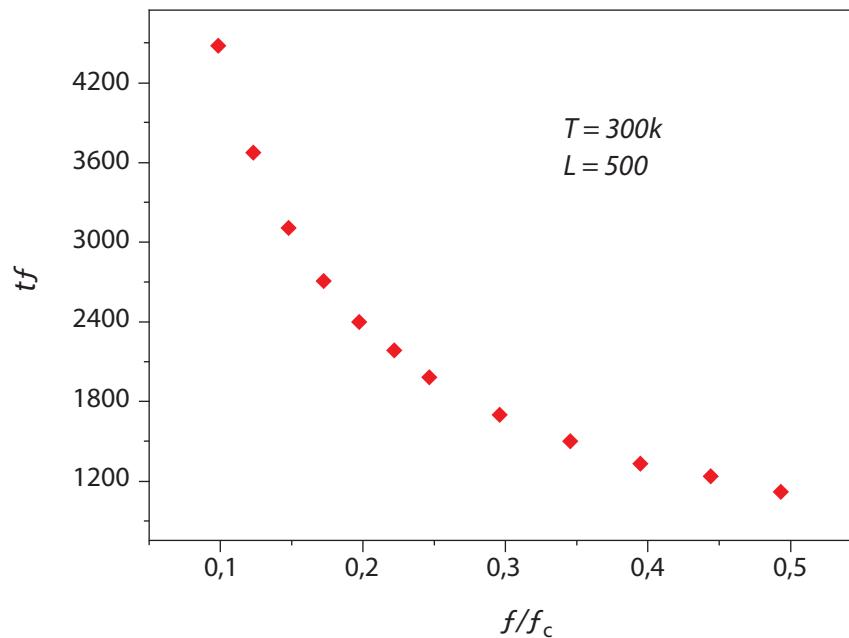
Fig 1: the lifetime versus applied load for system of seize *L=500*

To be able to investigate the crack diffusion created in the midst of the material, we have determinate the full time evolution of the region *A* of the damaged region versus both applied load *f* and temperature *T*. The corresponding answers are plotted in fig 2. The obtained results reveal that the damaged region increases with applied load and they are more consisting with the Lifshitz-Sloyosof law:

$$A = B(T)t^x \tag{5}$$

where *x* is crack diffusion exponent and *B* is a constant which depends only on the system temperature and related to the diffusion coefficient of the created crack by:

$$D \propto B(T)^{1/x} \tag{6}$$

So the calculated value of the diffusion exponent of the created crack is $x \approx 2$.
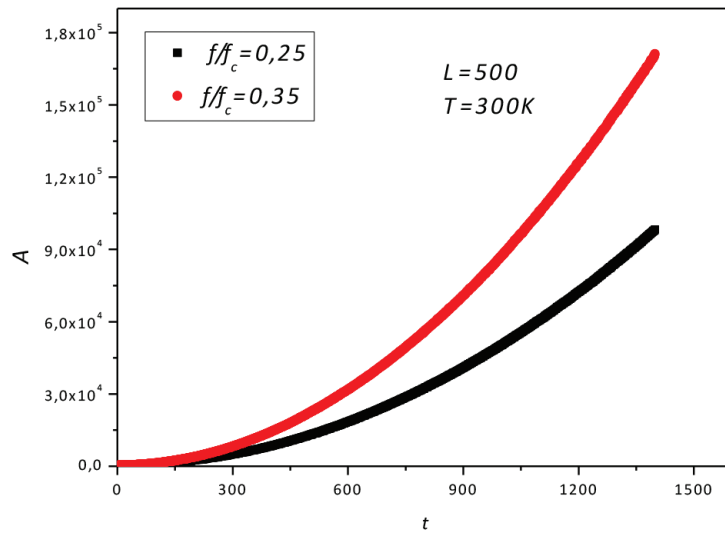
Fig 2: the time evolution of the era of the damaged region
for two different s value of the applied load

Utilizing the formula (6), we have determined the diffusion coefficient of the created crack versus applied load. The corresponding results are plotted in fig 3. Therefore, we are finding that the diffusion coefficient increases linearly with the applied load.
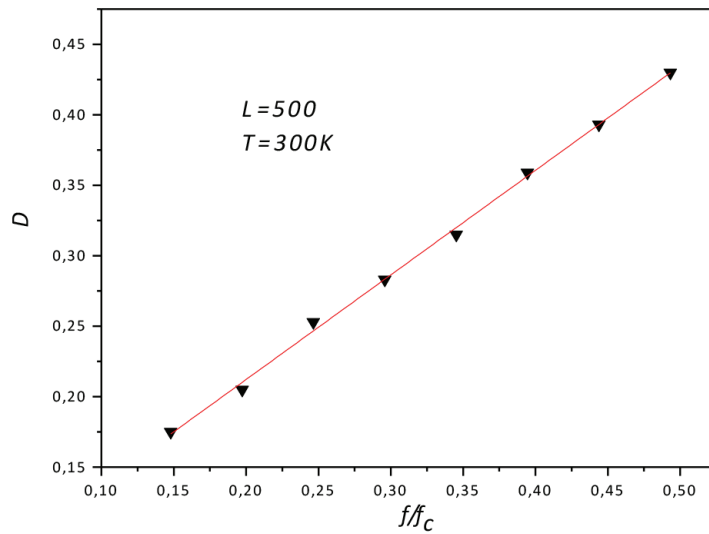
Fig 3: the diffusion coefficient versus
applied load for system of seize *L=500*

IV. CONCLUSION

To sum up, we have investigated the crack diffusion created at single point of the composite materials by using the fiber bundle model in the local load sharing rule. So, we have considered a fiber bundle on which we have applied an external load at a single point, and we then continue to increase this load at a very slow rate until the centered fiber breaks and its load is redistributed to its neighboring intact fibers. This breaking and redistribution dynamics repeat itself and this process ensures an advancing interfacial fracture and the area of the damaged region increases with time until a final crack of material. The equivalent effects display that place reveals a Lifshitz-Sloyosof law with an exponent growth $x=2$. The discovered law enables us to deduce the conduct of the crack diffusion coefficient. We are finding that the developed split in the midst of the material rises linearly with used fill.

References

[1]   F.Raischel, F. Kun, H.J. Herrmann, Phys. Rev. E 73, 066101(2006).

[2]   A. Hader, Y. Boughaleb, I. Achik1 and K. Sbiaai. Opt.Mat. 36, 3-7(2013).

[3]   A. Lahyani, Y. Boughaleb, M. Qjani, S. Ouaskit and R. El Guerjouma, Mediterranean Journal of electronics and communications. 6, 23-26 (2010).

[4]   SO. Ramas,P.-P. Cortet, S. Cilibreto and Vanel, Phys.Rev.Lett.110, 165506(2013).

[5]   O. Ramas,P.-P. Cortet, S. Cilibreto and Vanel, Phys.Rev.Lett.110, 165506(2013).

[6]   D. Amitrano, Eur. Phys. J.B. Special Topics 205, 199-215(2012).

[7]   S. Pradhan, A. K. Chaudra, Bihas K. Chakrabarti, Phys. Rev. E. 88, 012123 (2013).

[8]   S. Pradhan, A. Hansen, and P. C. Hemmer, Phys. Rev. Lett. 95, 125501 (2005); Phys. Rev. E 74, 016122 (2006).

[9]   A. Hader, I. Achik, K. Sbiaai, Y. Boughaleb, Superlattices and Microstructures S0749-6036(2014)00087-1.

[10] S. Pradhan and B. K. Chakrabarti, Phys. Rev. E 65, 016113 (2001); S. Pradhan, P. Bhattacharyya, and B. K. Chakrabarti, Phys. Rev. E 66, 016116 (2002); P. Bhattacharyya, S. Pradhan, and B. K. Chakrabarti, Phys. Rev. E 67, 046122 (2003).

[11] H. A. Daniels, Proc. R. Soc. London A 183, 405 (1945).

[12] F. T. Peirce, J. Text. Ind. 17, 355 (1926).

[13] H. E. Daniels, Proc. R. Soc. London Ser. A 183, 405 (1945).

[14] R. L. Smith, Ann. Probab. 10, 137 (1982).

[15] S. L. Phoenix and R. L. Smith, Int. J. Solids Struct. 19, 479 (1983).

[16] D. Bonamy and E. Bouchaud, Phys. Rep. 498, 1 (2011).

[17] A. Delaplace, J. Schmittbuhl, and K. J. M°aløy, Phys. Rev. E 60,1337 (1999).

[18] Qiming Li, M.C.Tringides, Surf. Sci 365, 495 (1996).

[19] K. Saadouni, A. Hader, A. Jaouad, Y. Boughaleb Surf. Sci 572, 366 (2004).

Comparison of MPPT techniques:
"P&O" and "InCd" for PV systems

S. Hakim[1], M. Elyaqouti[2], S. Farhat[2], L. Bouhouch[2] and A. Moudden[1]

[1] LMTI, Faculty of Sciences of Agadir (FSA),
University Ibn Zohr, BP 8106, Agadir, Maroc

[2] ERTAIER, Superior school of Technology (EST), BP 33/S, Agadir, Maroc

Corresponding author E-mail: safa.hakim@edu.uiz.ac.ma

Abstract. *The energy utilization efficiency of the photovoltaic can be significantly improved by employing the MPPT (Maximum power point trackers) method. The MPPT is one of the key technologies in photovoltaic generation system;it allows extraction of maximum available power from the photovoltaic (PV) array.The maximum available power is tracked using specialized algorithms such as Perturb and Observe (P&O), and Incremental Conductance (InCd), which are widely applied in the MPPTcontroller due to their simplicity and easy implementation. This paper presents a detailed comparison of their theories and their simulations under the Matlab / Simulink environment. The obtained results show that the use of MPPT control improves in a considerable way the performance of PV systems.*

Key words: DC-DC power conversion; Matlab/ Simulink; Maximum Power Point Tracking (MPPT); Photovoltaic (PV) power systems.

1. Introduction

With the increasing demand of electrical energy and the rise of the global warming, it is natural that scientific research is increasingly oriented towards renewable energies development [1]. These technologies have an important role in solving the mentioned greatest issues [2].

Nowadays it is an indisputable fact that people are obliged to cover their continuously increasing energy needs with new, inexhaustible, and environmentally friendly electric power sources[3]. Among of renewable sources, PV generation is gaining increased importance and has become quite popular thanks to inherent advantages like absence of fuel cost, no noise and wear due to absence of moving parts, little maintenance and not producing any green house gasses[4].So the PV is an attractive source of energy. Abundant and ubiquitous, this source is one of the most important renewable-energy sources that have been increasing worldwide year by year[5].

However, a simple system configured with PV generator (PVG) presents production loss because it does not operate at the maximum power point (MPP). To solve this problem it is possible to insert a DC/DC converter between the PVG and the load. This latter, besides the typical functions assigned to the controllers, it can control the seeking of the MPP. This converter is named MPPT system [6].

Several MPPT techniques have been proposed in the literature, such as "*Perturb and Observe*", "*Incremental Conductance*", "*Parasitic Capacitance*", "*Constant Voltage*", and "*Artificial intelligence techniques*". These methods vary in their simplicity, convergence speed, and hardware implementation [7].On the

one hand, conventional methods, as "Perturb and Observe", guarantee acceptable performances, and are easy to implement. On the other hand, artificial intelligent methods perform better but are generally more complicated to implement; they also require relatively high performance of control processor [5].

Our paper is organized as follows: after an introduction, a brief description of photovoltaic and modeling of the system are presented in section 2. Section 3 describes the implementation of the chosen MPPT algorithms; "P&O" and "InCd". Results and discussions are given in section 4. Finally, we conclude our investigations in section 5.

2. System modeling

There are multiple ways of achieving impedance matching for the solar panel to the load: a general diagram is presented in Fig. 1. The system is composed of a MPP computing device and a DC-DC converter.
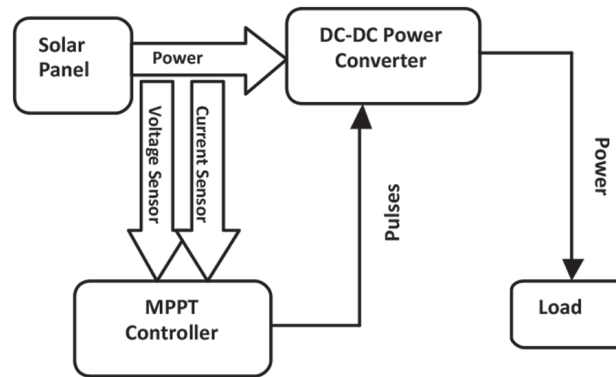
Figure 1: Block diagram of the proposed PVG system.

2.1. PV panel model

The PV panel studied in this paper is Kyocera KC40 [8] that is installed in ERTAIER laboratory (Research team in Advanced Technologies and Engineering of Renewable energies located at University of Technology of Agadir). Table 1 summarizes the used electrical characteristics and parameters for modeling the PV panel:

Parameter	Value
Open circuit voltage V_{oc}	21.5 V
Maximum power voltage V_m	16.9 V
Short circuit current I_{sc}	2.48 A
Maximum power current I_m	2.34 A
Maximum power P_m	40 W

Table 1: PV cell's parameters

A solar cell is a basic building block of a PV system. Normally, a small solar cell generates about one watt. A group of solar cells are connected in series and parallel circuits to generate high power and this combination is called PV panel.

The PV cell can be represented by the electrical model shown in Fig. 2. This model consists of a current source, a diode D, and a pair of resistors.
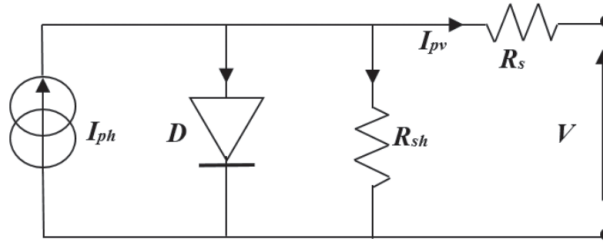
Figure 2: Equivalent circuit diagram of a solar cell

The *I-V* characteristic of PV cells is expressed by the following equation (1). Sometimes, to simplify the model, the effect of the shunt resistance is not considered, i.e. R_{sh} is infinite, so the last term in (1) is neglected.

$$I = I_{ph} - I_s \left(\exp\left(\frac{q(V + R_s I)}{nKT} \right) - 1 \right) - \frac{V + R_s I}{R_{sh}} \qquad (1)$$

Where:

Parameter	
I, V	Current and Voltage of PV cell (A)
I_{ph}	PV generated current (A)
I_s	Diode saturation current (A)
q	Electronic charge (= 1.6 10^{-19} C)
n	Diode ideality factor
K	Boltzmann's constant (= 1.38 10^{-23} J/K)
T	The solar array panel absolute temperature (°K)
R_s, R_{sh}	Serial and Parallel resistor

Table 2: Equation's parameters

2.2. Static converter Boost type's

The converter is used to increase the output voltage, compared to that delivered by the source; its simplest form is shown in scheme of Fig. 3. In the reference [9], the authors present the design method of boost converters. The table 3 summarizes the parameters values used by these authors.
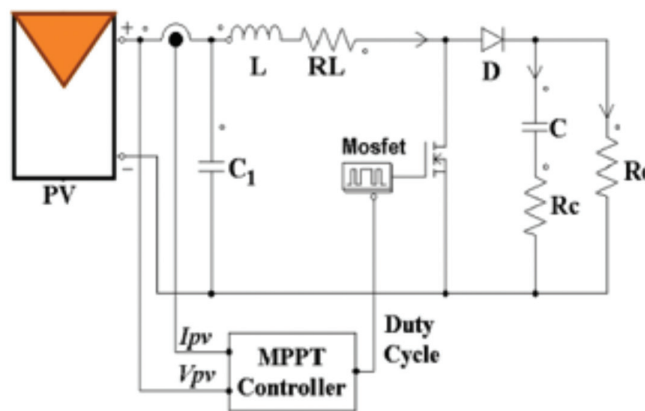
Figure 3: Diagram of the Boost converter

Boost Converter	Condenser C	7.5 mF
	Inductor L	50 mH
	Resistor R_c	0 W
	Resistor R_L	1 W
Condenser of Coupling	Condenser C_1	440 nF
Load	Resistor R_o	12 W

Table 3: Parameters of Boost converter

3. MPPT algorithms

3.1. "P&O" command

The most commonly used MPPT algorithm is "P&O" (Perturb and Observe), due to its ease of implementation in its basic form.Thus, if the operating voltage of the PV array is perturbed in a given direction and $dP/dV > 0$, it is known that the perturbation has moved the PV panel operating point toward the MPP. The P&O algorithm would then continue to perturb the PV array voltage in the same direction. If $dP/dV < 0$, then the change has moved the operating point of PV panel, away from the MPP, and the P&O algorithm reverses the direction of the perturbation.A problem with P&O is that it oscillates around the MPP in steady state operation. It also can track in the wrong direction, away from the MPP, increasingly rapidly when the irradiance levels increases or decreases. There are several variations of the basic P&O that have been designed to minimize these drawbacks[10].

3.2. "InCd" command

The incremental conductance algorithm seeks to overcome the limitations of the P&O algorithm by varying a PV panel's incremental conductance to compute the sign of dP/dV without a perturbation.The incremental conductance algorithm is derived by differentiating the PVpanel power with respect to voltage (dP/dV), and setting the result equal to zero ($dP/dV = 0$).Beginning with this condition, it is possible to show that, at MPP the $dI/dV = -I/V$. Thus, the MPPT based on incremental conductance achieves the MPP and stop disturbing the operating point. If the condition is not met, the relationship between dI/dV and $-I/V$ can be used to determine the direction in which the voltage must be changed in order to reach the MPP.This relationship is deduced from the fact that dP/dV is negative when the operating point is to right of "MPP" and positive when it's to the left of "MPP"[10].

"InCd" algorithm has advantages over "P&O" in that it can determine when the operating point has reached the "MPP", whereas "P&O" oscillates around the MPP. Also, "InCd" can track rapidly the increasing, and decreasing irradiance, with higher accuracy than "P&O" without oscillations. One disadvantage of InCd algorithm is his increased complexity when compared to "P&O". This leads at an increases in computational time, and slows down the sampling frequency of the PV panel voltage and current [10].

4. Results and interpretations

Figures 4 and 5 show that the current and the power extracted at a fixed temperature ($T = 25$ °C), increase proportionally with the solar flux. Indeed the maximum power is very sensitive to the variations of irradiation.
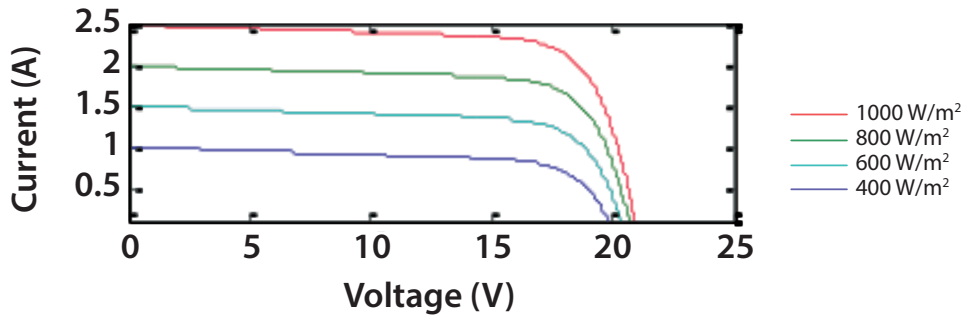
Figure 4: Current-voltage characteristics *I*(*V*)
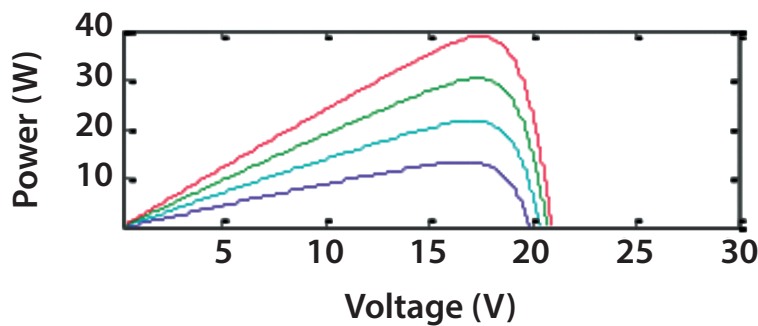
Figure 5: Power-voltage characteristics P(V)

After several tests, for example for radiation (G = 1000 W/m2), and at ambient temperature (25 °C), the simulations results of the power provided by the PVGshown in Fig. 6 show that the system converges quickly towards maximum power point (MPP) after a less than 240 ms, applying MPPT algorithm using the controller «P&O» and after 450 ms in the case of the controller «InCd».

Once the desired «MPP» is reaches, the controller oscillates around the MPP. We noted also that the «P&O» method produces oscillations around the MPP. While the «InCd» technique has the advantage over the «P&O» method that it can reach the MPP without oscillating around this value. So the technique «InCd» is much more stable.But «P&O» has the potential to be very competitive with other methods, if it is properly optimized and leads to an efficiency which is equal to that obtainable by the «InCd» method.
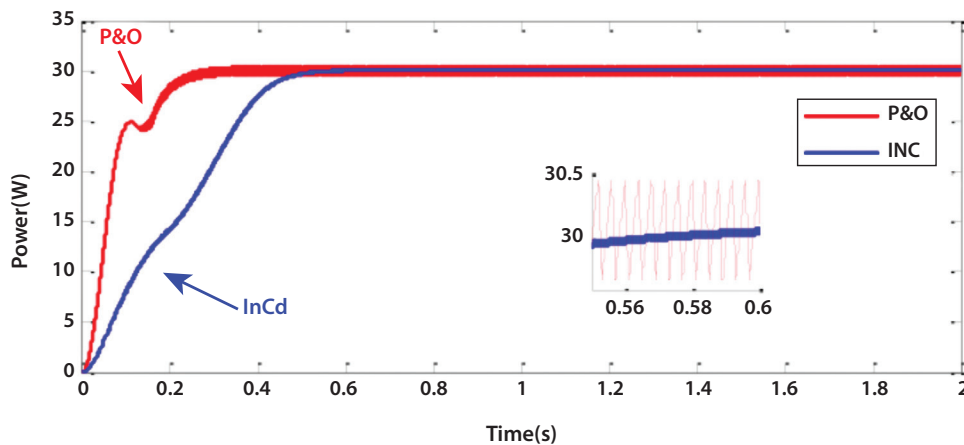
Figure 6: Comparison between "P&O" and "InCd" techniques

In order to validate our results, we compared our simulations with experimental results obtained by my colleagues [11] in our ERTAIER laboratory, using a DAQ acquisition card. Figure 7 summarizes the obtained results.

Experimental Result for G=1000 w/m² and T=26 °C
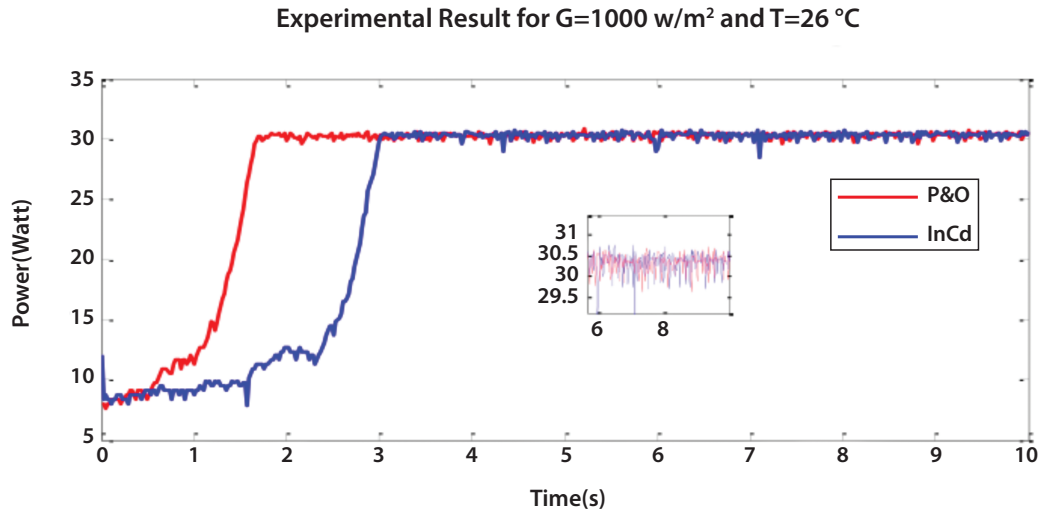
Figure 7: Comparison between the experimental results of "P&O" and "InCd" techniques [11]

We can deduce that this experience confirms the simulation results that we have obtained. We note that the practical response time is slightly larger to the simulated; this is probably due to the time of acquisition and processing of the acquired data on the card.

5. Conclusion

In this work, we have studied and analyzed, by modeling and simulating under Matlab/Simulink, the operation of a PV system. The latter has a load controlled by a Boost converter. The control is provided by two types of MPPT control which are "P&O" and "InCd".The obtained results based on simulations and experimental validation, show that the use of MPPT control improves in a considerable way the performance of PV systems.

A comparison between the two algorithms confirms that there is a significant improvement in stability around the PPM by using the "InCd". Indeed, we note that the technique "InCd" is much more stable, because we have observed that the "P&O" method produces oscillations around the MPP, whereas the "InCd" technique can reach the MPP without oscillations. However, it happens that the"P&O" method, when properly optimized, can have MPPTefficiencies well in excess of 97%,and is highly competitive against other MPPT algorithms.

References

[1] Dorin Petreuş, Toma Pătărău, Stefan Dărăban, Cristina Morel, Brian Morley, A novel maximum power point tracker based on analog anddigital control loops, Solar Energy, Vol. 85, Issue 3, (2011), pp. 588-600.

[2] S.A.KH. Mozaffari Niapour, S. Danyali, M.B.B. Sharifian, M.R. Feyzi, Brushless DC motor drives supplied by PV power system based on Z-source inverter and FL-IC MPPT controller, Energy Conversion and Management Vol. 52, Issues 8-9, (2011), pp. 3043-3059.

[3] Sotirios B. Skretas, Demetrios P. Papadopoulos, Efficient design and simulation of an expandable hybrid (wind–photovoltaic) power system with MPPT and inverter input voltage regulation features in compliance with electric grid requirements, Electric Power Systems Research, Vol. 79, Issue 9, (2009), pp. 1271-1285.

[4] S.M. Ali, Punyashree Pattanayak, Prasun Sanki, R.R. Sabat, Modeling and control of grid-connected hybrid photovoltaic distributed generation system,IJESET, ISSN: 2231–6604, Vol. 4, Issue 1, (2012), pp. 125-132.

[5] A.Mellit, H. Rezzouk, A. Messai, B. Medjahed, FPGA-based real time implementation of MPPT-controller for photovoltaicsystems, Renewable Energy,Vol. 36, Issue 5, (2011), pp. 1652-1661.

[6] V. Salas, E. Olıas, A. Lázaro, A. Barrado, Evaluation of a new maximum power point tracker (MPPT) applied to the photovoltaic stand-alone systems, International Conference on Physics, Chemistry and Engineering, Solar Energy Materials and Solar Cells,Vol. 87, Issues 1-4, (2005), pp. 807-815.

[7] Nacerk M'Sirdi, Abdelhamid Rabhi, Mouna Abarkan, A new VSAS approach for maximum power tracking for renewable energy sources (RES), Energy procedia 42, (2013), pp. 708-717.

[8] KYOCERA Corporation, KC40, High Efficiency Multicrystal Photovoltaic Module, http://www.kyocerasolar.com/assets/001/5158.pdf

[9] M. Meddah, M. Bourahla, N. Bouchetata, Synthèse des convertisseurs statiques DC/AC pour les systèmes photovoltaïques,Revue des Energies Renouvelables, ICESD'11, Adrar, (2011), pp. 101112.

[10] D.P. Hohm, M.E. Ropp, Comparative Study of Maximum Power Point Tracking algorithms,Progress in Photovoltaics: Research and Applications,Vol. 11, Issue 1, (2003), pp. 47-62.

[11] S. Farhat, R. El Moutawakil Alaoui, L. Bouhouch, A. Ihlal, P&O and InC Implementation, accepted in IREE journal, (March 2015).

Study of the diffusion mechanisms and the growth thin film of aluminum on Ni(100) substrate by molecular dynamics

A. Hassani[1,*], A. Makan[2], K. Sbiaai[3,], A. Tabyaoui[1], A. Hasnaoui[3]**

[1] Laboratory of Radiation and Matter, Faculty of Science and Technology,
University Hassan 1er, 26000 Settat, Morocco.

[2] Laboratory of Water and Environment, Faculty of Science,
University Chouaib Doukkali, El Jadida, Morocco.

[3] Univ Hassan I, Laboratoire de sciences de matériaux, milieu et de la modémisatin (LS3M),
Faculté Polydisciplinaire de Khouribga, 25000 Khouribga, Morocco.
Corresponding authors : a.hassani.uh1@gmail.com/ksbiaai@gmail.com

Abstract

Molecular modeling does not replace experimental or theoretical methods previously developed, but provide an additional tool for material behavior understanding. The method of molecular dynamics is one of several existing modeling methods to better understand the dynamics at atomic or molecular scale. Embedded Atom Method (EAM) was adopted in this study to solve the N-body problem. The purpose of this investigation was the study of different growth mechanisms and morphology of Al-thin film on Ni(100) substrate at 300 K. In this context, several simulations were performed using the Pun and Mishin potential. We explored some diffusion mechanisms that occurred during the layers formation, namely the jump and the exchange mechanisms that influence the growth mode of the film and the roughness of the formed surface.

Keywords: Molecular dynamics, film growth, jump diffusion, exchange mechanism,

1. Introduction

Thin film is one of the manufacturing technic, which recognized a huge expansion in the sector of high tech industries; namely photovoltaic cells [1], microelectronic devices [2], biomedical [3], aerospace [4], and smart materials [5]. Elaboration of the thin film is made by layers deposition, whether by catholic sputtering or vacuum evaporation. To conceive new materials with high performance requires understanding different phenomena that can occur at the atomic scale (diffusion, exchange...). The energy and angle of incidence of deposited atoms [6,7] as well as temperature of the substrate [8] on which atoms are deposited are potential parameters which play a very important role in thin film deposition processes and can be controlled depending on the system. Moreover, diffusion mechanisms of deposited atoms on the surface, which cannot be controlled, determine the morphology of the thin film growth [9-13]. However, it is extremely difficult to understand, experimentally, these mechanisms due to the insufficient experimental method to analyze thin-film morphology on the atomic scale. On the other hand, the molecular dynamics (MD) simulation method has been successfully adapted to investigate the growth mechanism of various kinds of thin films [14-18].

The system formed by Ni and l was attracted the attention of scientific community in recent year. In this context, our attention has focused in such system in order to more understanding the thin film growth process in both nickel and aluminum systems. It is worth to mention that our investigation are made on homo and heterogeneous systems. On the other hand, we note that nickel and aluminum, and their alloys, have a large application in technical sectors such aviation construction and others.

It's known that the molecular dynamics method is capable to simulate, precisely, the nano-scale thin film nature and characteristics. For this purpose, molecular dynamics method was used to investigate the thin film growth and diffusion mechanisms of aluminum on Ni(100) substrate, according to substrate temperature of 300K and adatom incident energy of 1 eV.

2. Simulation method

A molecular dynamics (MD) scheme based on the embedded atom method (EAM) was adopted to simulate the required atomic interactions. The Ni-Al potential developed by G.P. Purja Pun and Y. Mishin [19] was used in this work because it has demonstrated a fairly good agreement with experimental data for the formation energies of several compounds of the Ni-Al system and it has proved its compatibility with the LAMMPS code [20] across several studies of the Al-Ni systems [21,22].
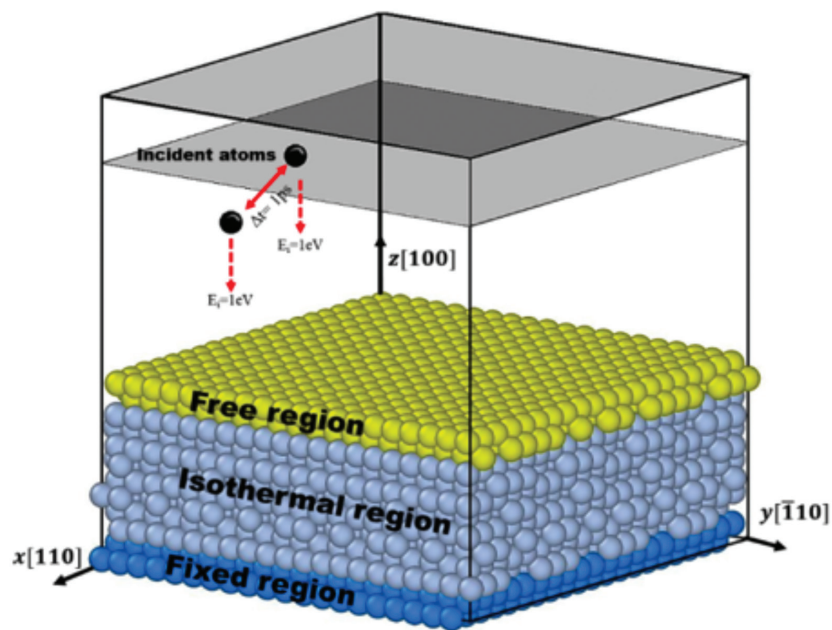
Figure 1: Atomic configuration of Ni(001) substrate employed for MD simulation

The cutoff distance, r_c, of all potentials was set to 6 Å. The size of fcc-Ni(100) substrate was prepared to be 49.7803 Å × 49.7803 Å × 21.12 Å in the orthogonal reference , and respectively, with the surface perpendicular to the z-axis. The substrate contained 12 layers (400 atoms/layer) (see Fig.1). The periodic boundary conditions were used in both x and y directions. The substrate was composed of one fixed region at the bottom, which was fixed at 0K to prevent the substrate from drifting; a second isothermal region which was set to absorb the kinetic energy of incident atoms and latent heat of condensation; and a third free region at the top surface to enable deposition on it. Before deposition, the substrate was relaxed at T = 300K for 40 ps (Fig.2). The Al atoms were added at a distance of 40 Å from the substrate surface with incident energy of 1eV. Accordingly, in this study, the MD time step was set to 1 fs and the system was fully relaxed for each additional adatom to reach equilibrium in the limit of 1 ps.
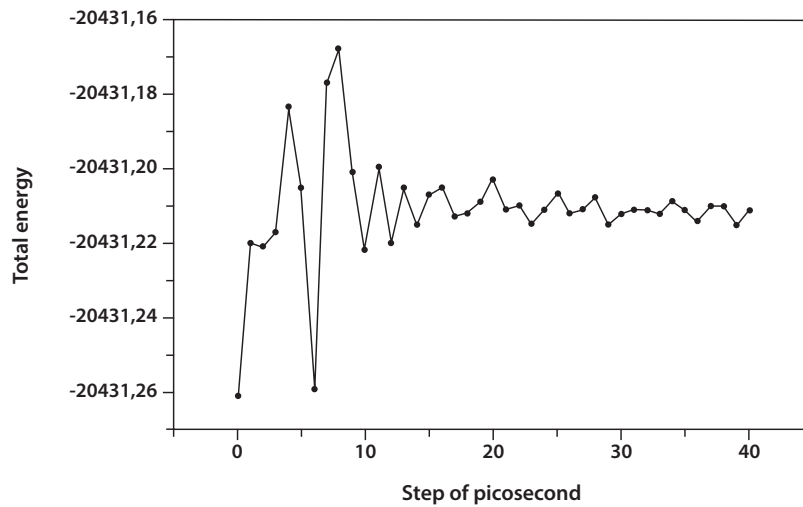
Figure 2: Substrate relaxation for 40ps

3. Results and discussion

In this study, we deposited 3600 Al atoms on Ni (100) substrate as shown in Fig.3. The 12 layers of Ni contain 400 atoms each of square structure.
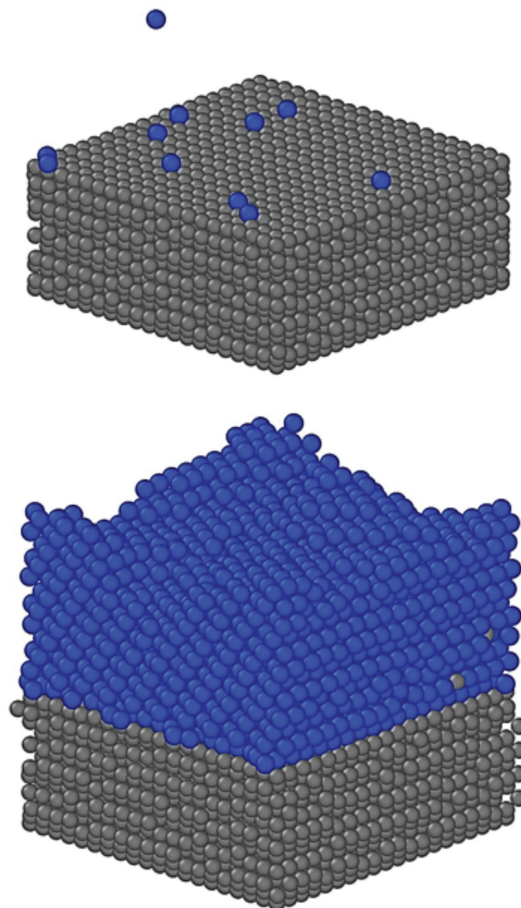
Fig.3: Deposition of 3600 Al atoms on Ni(001) substrate

The method of deposition of Al atoms occurs atom by atom. The deposited atom on the surface makes several diffusion processes. We observed that the Al adatom diffuse through mechanisms such as jump and exchange mechanism. These diffusion mechanisms allow Al adatoms to connect with each other and form aggregates (small clusters), the number of atoms is greater than or equal to 2. The Fig.4 illustrates the diffusion process as a mechanism for jumps, where adatom 1 passes from an hollow site to another near neighbor site. Such process is widely observed in various systems such as homogeneous systems [23,13] and heterogeneous systems Ag/Cu (110), Cu/Ag (110) [24,25,26,27]. Furthermore, jump mechanisms contribute horizontally to the layer growth in the (x,y) plane.
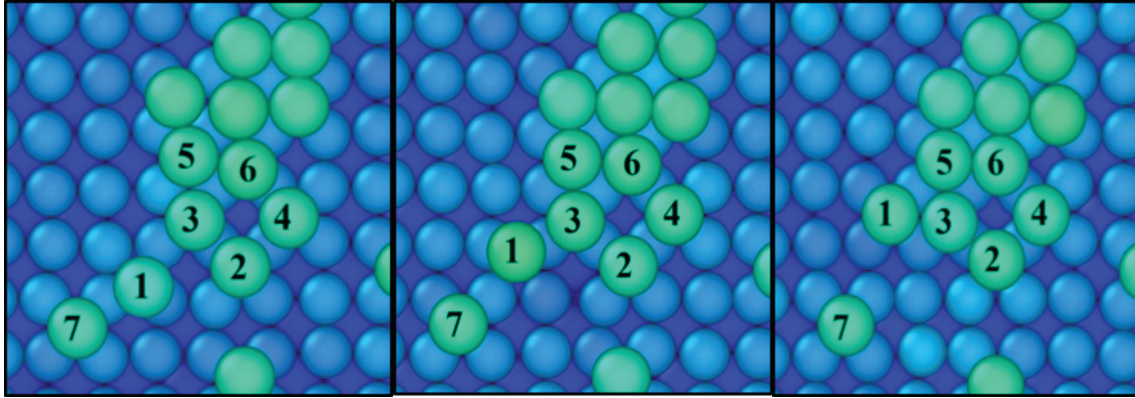
Fig.4: Diffusion through a jump mechanism

The exchange phenomenon is a phenomenon that allows the adatom to integrate surface and become an integral part of it [28]. In the case of our system, this mechanism is illustrated in Fig.5. The incident atom 1 was settled in a hollow site from an aggregate formed by atom 2, 3, 4 and 5. Then, the atom 2 was diffused to another near neighbor hollow site allowing the exchange with the atom 1, which integrates the aggregate surface. Moreover, the number of exchange mechanisms, that takes place in the surface, influences the film morphology and then the mode growth which dictate the roughness of the system.
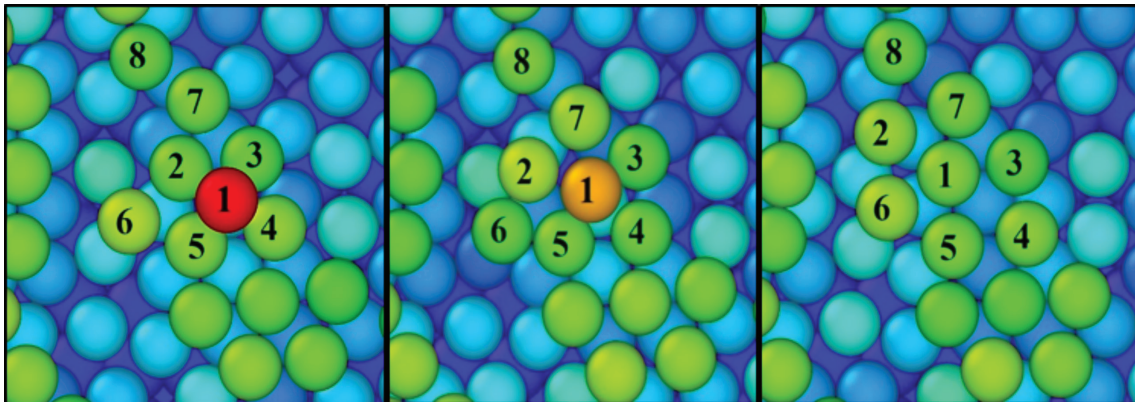
Figure 5: Illustration of the phenomenon of exchange

4. Conclusion

The molecular dynamics simulation was used in this study based on the model of the atom surrounded (Embedded Atom Method-ASM) to solve the many-body problem. We explored some diffusion mechanisms that occurred during the layers formation, namely the jump and the exchange mechanisms. We found that the jump mechanisms contribute horizontally to the layer growth in the (x,y) plane. Moreover, the number of exchange mechanisms, that takes place in the surface, influences the film morphology and then the mode growth which dictate the roughness of the system.

References

[1]   Peter Peumans, Soichi Uchida & Stephen R. Forrest, Nature, 425 (2003) 158-162.

[2]   Davis, Robert F, Kelner, G. ; Shur, M. ; Palmour, J.W. Browse Journals & Magazines > Proceedings of the IEEE, Volume:79 Issue:5

[3]   Kayano Sunada, Yoshihiko Kikuchi, Kazuhito Hashimoto, and Akira Fujishima, *Environ. Sci. Technol.* (1998), 32(5), pp 726-728

[4]   Martin, L.C.; Wrbanek, J.D.; Fralick, Gustave C. Instrumentation in Aerospace Simulation Facilities (2001). 19th International Congress on ICIASF 2001

[5]   Self-cleaning method for plasma CVD apparatus Hideaki Fukuda 3 nov. 2005 Numéro de publication US20050242061 A1

[6]   Yongzhi Cao, Junjie Zhang, Tao Sun, Yongda Yan, Fuli Yu. Applied Surface science, 256 (2010), 5993-5997

[7]   Yongzhi Cao, Junjie Zhang, Chao Wu, Fuli Yu. Thin Solid Films 544 (2013) 496-499

[8]   Y.Y. Cheng, C.C. Lee. Surface & Coatings Technology 203 (2008) 918–921

[9]   A. Zangwill, Physics at Surfaces (Cambridge University Press, Cambridge, UK, 1988).

[10] E. Kaxiras, Comput. Mater. Sci. 6, 158 (1996)

[11] C.L. Liu a, J.M. Cohen b, J.B. Adams a and A.F. Voter b Surface Science 253 (1991) 334-344

[12] A. Bilic´, B.V. King, D.J. O'Connor. Surface Science 442 (1999) 256–264

[13] Syed Islamuddin Shah, Giridhqr Nandipati, Abdelkader Kara, and Talat S.Rahman PHYSICAL REVIEW B 88, 035414(2013).

[14] S.-P. Kim, Y.-C. Chung, S.-C. Lee, K.-R. Lee, K.-H. Lee, J. Appl. Phys. 93 (2003) 8564.

[15] S.-G. Lee, Y.-C. Chung, J. Korean Phys. Soc. 47 (2005) S585.

[16] S.-G. Lee, Y.-C. Chung, J. Appl. Phys. 100 (2006) 074905.

[17] R.W. Smith, D.J. Srolovitz, J. Appl. Phys. 79 (1996) 1448.

[18] S-G Lee, Y-C Chung, Applied Surface Science 253 (2007) 8896–8900

[19] M. Ludwig and P. Gumbsch, Modell. Simul. Mater. Sci. Eng. 3 (1995) p.533.

[20] Y. Mishin, Acta Mater. 52 (2004) p.1451.

[21] Y. Mishin, M.J. Mehl and D.A. Papaconstantopoulos, Phys. Rev. B 65 (2002) p.224114.

[22] G.P. Purja Pun and Y. Mishin, Phil. Mag. 89, 3245 (2009).

[23] C.L. Liu, J.M. Cohen, J.B. Adams and A.F. Voter. Surface Science, 253 (1991) 334-344

[24] K. Sbiaai, Y. Boughaleb, M. Mazroui, A. Hajjaji, A. Kara Thin Solid Films, 548, 331-335 (2013).

[25] K. Sbiaai, Y. Boughaleb, J.Y. Raty, A. Hajjaji, M. Mazroui, A. Kara. Journal of Optoelectronics and Advanced Materials Vol. 14, 1059 (2012)

[26] Elkoraychy, Elyakout; Sbiaai, Khalid; Mazroui, M'hamed; Boughaleb, Yahia; Ferrando, Riccardo, Surface Science, 635, 64-69 (2015).

[27] K. Sbiaai, El. ElKoraychy, M. Mazroui, and Y. Boughaleb Accepted in surface and interface analysis (2015).

[28] Khalid Sbiaai. Journal of Optoelectronics and Advanced Materials, Vol 15, 501-504 (2013).

A New and simple pathway route way for the synthesis of silver nanoparticles using the industrial latex

A. Eddahbi[1], A. Moumen[1], M. Ider[1], S. Ouaskit[1], K. Abderrafi[2] and A. Dezairi[1]

[1] Laboratoire de Physique de la Matière Condensée LPMC,
Unité de recherche associée au CNRST (URAC10)

[2] Instituto de Microelectronica de Madrid (IMM) Isaac Newton 28760 trescantosmadrid, Spain

Université Hassan II- Mohammedia. Faculté des Sciences Ben M'Sik, B.P. 7955, Casablanca, Morocco.
e-mail: s.ouaskit@ipnl.in2p3.fr(eddahbi-adil@hotmail.com)

Keywords: Silver nanoparticles, latex, microwave process, self-assembly method, encapsulation.

Abstract. *This paper presents a new method for preparing silver nanofluids based onself assembly process induced by the aqueous emulsion of copolymers (Latex) on Silver nitrate precursor dissolved in alcohol. We have observed after few hours, that nanoparticles of silver are formed in the alcohol/latex solution without need of any external thermal excitation. These results are compared with the case where the synthesis was assisted by microwave providing thermal excitation.*

The latex polymers act as reducer inducing Ag+ →Ag° reaction in the colloidal solution and also as the protecting agent of the formed Ag nanoparticles encapsulated in the latex matrix. The obtained solutions have been characterized by The UV-Visible, XRD, TEM, and SEM. The UV- Visible spectrum shows a single peak at 425 nm arising from the surface plasmon absorption of silver nanoparticles. The TEM results showed that the spherical particles had an average diameter of 7 nm. The synthesized samples prepared Ag NPs were stable for more than 12 months at room temperature.

1- INTRODUCTION

Metal nanoparticles have attracted extensive research interest because of their unique size dependent optical [1] and electronic properties [2]. Among the noble metal nanoparticles, silver has got much recognition due to its potential applications in various fields such as photonics [3], microelectronics [4], photo catalysis [5], lithography [6], biosensor material [7], etc. Also silver nanoparticles are known for their antimicrobial properties [8] and even have shown to prevent HIV binding to host cells [9]. Since, these properties strongly depend on shapes and sizes of nanoparticles, extensive studies have been carried out on the shape and size controlled syntheses of metallic nanoparticles.

Aqueous emulsions are heterogenic phase systems in which stable nanodroplets of one phase are dispersed in a second, continuous phase polymer particles prepared as synthetic emulsions and latexes are frequently applied as binders in the industrial fields of paint, paper and inks, and films such as adhesives and coating materials.

Those emulsions are prepared of nano to micron-sized polymer particles by radical polymerization of vinyl monomers in environmentally friendly heterogeneous aqueous media. Consequently, considerable

attention has recently been directed towards aqueous dispersed systems due to the increased awareness of environmental issues. Moreover, such polymer particles have already been applied to more advanced fields such as biotechnology where latexes have many potential biomedical applications such as controlled-release drug-delivery [10,11], biocatalysis applications [12,13], fluorescent-dyed latex particles [14] are also used in fluorescence microscopy, and DNA analysis applications.

The interest in the field of electronic technologies of latex in nanofabrication is increasing in designing regular structures in the nanoscale range which have relevant optical [15] and electrical [16] properties for optoelectronic devices such as sensors [17].

Nanostructured materials [18] can be produced using latex particles as templates to obtain a nano sized polymer particles with uniform diameters which are arranged into regular structures upon drying [19].

In addition to the commercial interest of latex and emulsion, it is of fundamental scientific interest to elucidate the interest of those systems related to the fact that each of the nanodroplets can be regarded as a nanoscopic, individual batch reactor. A whole variety of synthesis reactions at the nanometric scale can be performed in this kind of medium. Additionally, aqueous emulsions are also suited for the encapsulation of various solid or liquid materials.

Emulsion polymers are colloids, meaning that they consist of small, discrete particles dispersed in a continuous liquid media. Colloids have many unique and interesting properties as a result of their small size (typically less than 1μm and large interfacial area (typically greater than 104 cm2/cm3 latex) [20].

The interfacial free energy increase is substantial in colloids with small sizes and large interfacial areas. The minimization of interfacial free energy is thermodynamically favorable [21], and provides a strong driving force for aggregation. Droplets reduce interfacial area by coalescence into pools of monomer, and particles do the same by aggregation into masses of polymer [22, 23].

In this work we have sought to combine the advantages of the chemical reduction route, environment-friendly reagents, and the stabilization of the particles in a latex matrix, with the goal of synthesizing nanoparticles embedded in dielectric films. This work was also stimulated by the use of latex as commercial ship medium and a new template of nanoparticles elaboration.

2. EXPERIMENTAL

2.1. MATERIALS

All chemicals and materials used in this investigation were reagent grade materials, and were used as received. The latex (aqueous dispersion of copolymers: acetate/vinyl versatate). Silver Nitrate (99% purity) $AgNO_3$. The solvent used in the study is ethanol (EtOH).

The apparatus used for the preparation is a microwave Mars5 (System from company CEM).

2.2. EXPERIMENTAL CHARACTERIZATION TECHNIQUES

The optical properties of Ag nanoparticles were recorded using UV-Visible spectroscopy (spectrophotometer UV-3100 selecta) to correlate their optical properties with the size, shape of nanoparticles and their particle dispersion in the polymer matrix. The spectras were recorded using 1cm³ quartz cell.

Size and shape were determined using FEI TECNAI G microscope transmission electron microscope. The particles were carried out at an accelerating voltage of 120 kV. The samples were prepared for TEM analysis by placing a drop of the solution on a carbon coated copper grid and drying in air. The X-ray diffraction patterns (XRD) were recorded on BRUKER (ADVANCE D8) diffract meter using Cu Kα radiation (λ~0.15418 nm) operated at 50 kV and 100 mA.

The morphologies of these Ag-latex nanocomposites were observed by using scanning electron microscopy (SEM, FEI Quanta 200)

2. 3. PREPARATION SYNTHESIS OF NANOPARTICLE COMPOSITES (LATEX-SILVER)

2.3.1. Microwave Assisted Synthesis Method

Silver nanostructures have been synthesized by a microwave -method. In this synthesis process, the latex and $AgNO_3$ (0.005M) was added in 10 ml of an alcoholic solution. The latex copolymers act both as stabilizer and reducer inducing Ag+ → Ag° reaction.

The solution was placed in a microwave oven that was operated at the 100% power of 300W and frequency for 50 s. The colorless solution instantaneously turned to the characteristic pale yellow color, indicating the formation of silver nanoparticles. The sample was cooled at 20–25 ℃ temperature just after the reaction. The successful incorporation of silver nanoparticles in latex matrix was confirmed by the transmission electron microscope (TEM)

The advantage of microwave-mediated synthesis over the conventional heating is the improved kinetics of the reaction generally by one or two order of magnitude, due to rapid initial heating and the generation of localized high-temperature zones at reaction sites [24].

2.3.2. Self-assembly method

In a typical synthesis, latex (1ml) was dissolved (50 ml) Ethanol under magnetic stirring in order to obtain a colorless transparent latex solution. A solution of silver nitrate-ethanol (5mM, 50 ml) was prepared and added to the latex solution with continuous stirring for about 2 h to ensure well homogeneity of the solutions. Finally, the solution was kept in dark and at ambient. After few hours under conditions, the apparent color in the resulting sample Ag– Latex of light pale yellow was formed, indicating the formation of Ag-nanoparticles.

3. Results and discussion

Fig. 1(a) shows the dependence of Ag nanoparticles formation on the MW exposure time. We observe that the main part of the reaction, 95%, takes place within the first 35 s and it is practically finished after 50 s. Regarding to the absorption spectrum of the unirradiated (t=0s) for Ag-Latex , it can be seen that a nearly zero absorption in the wavelength range (300–800 nm).

When $AgNO_3$ precursor is embedded in latex matrix, the optical properties are the net result of the electronic transition of the two materials. One can see that a strong increase in the absorbance in the ultraviolet and visible regions i.e. in the spectral range 300–600nm the absorption coefficient of the samples was increased with the increasing of the irradiation dose. The appearance presence of this peak in the visible region is due to the surface plasmon resonance (SPR) nature of the Ag nanoparticles embedded in a dielectric medium [25]. The symmetric shape of the SPR peak features out the spherical shape and uniform distribution of Ag nanoparticles within the latex matrix.

Fig. 2 shows TEM images of latex -coated Ag nanoparticles and their corresponding size-distributions prepared in Ethanol in different irradiation time in the MW. Most of the silver nanoparticles obtained upon MW irradiation are spherical. The average diameters of Ag nanoparticles are about 7 nm.
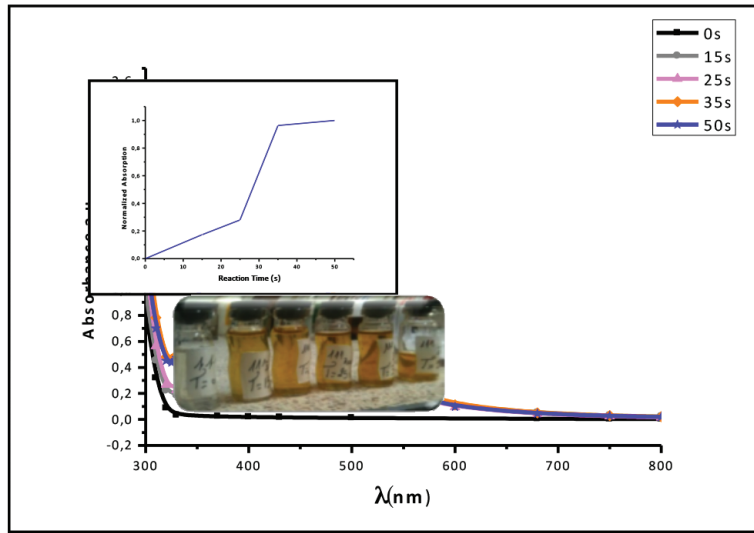
Fig .1. Absorption spectra of Ag nanoparticles for different MW irradiation times.
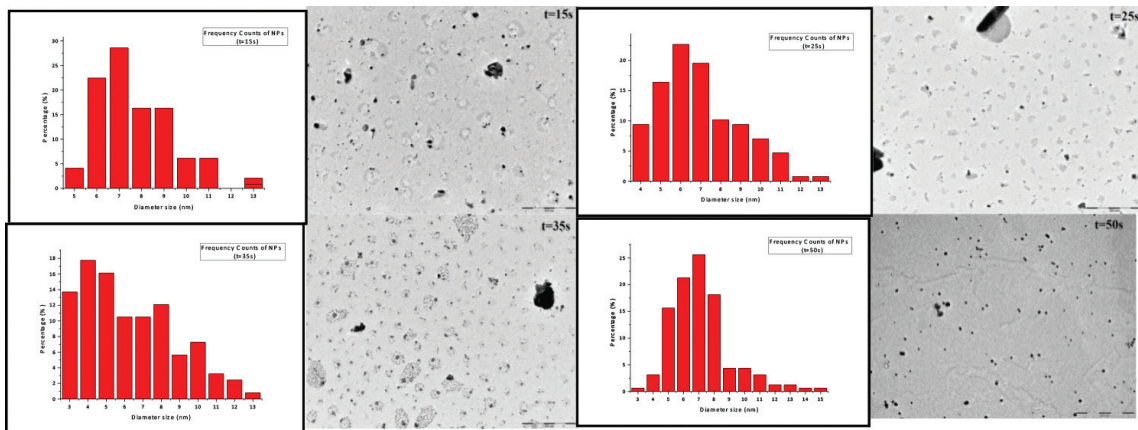
Fig.2 .TEM micrograph and size distribution of silver nanoparticles obtained at different MW irradiation times.
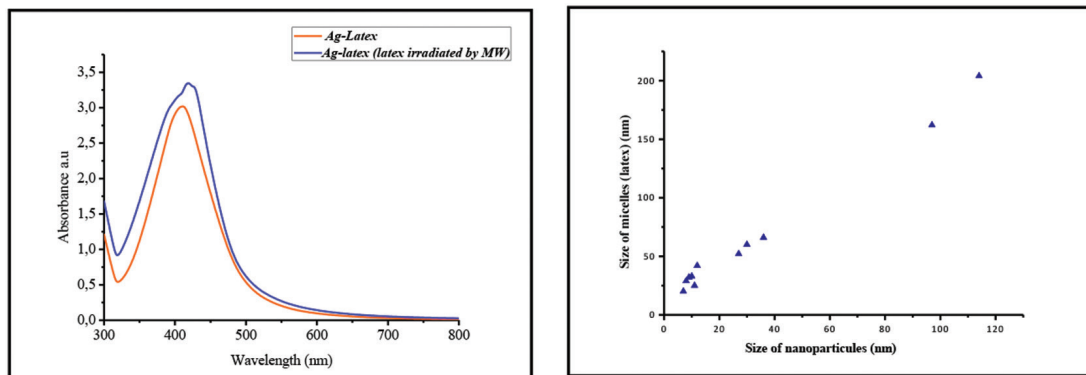
Fig.3. (a)/ UV-visible spectra of silver nanoparticles produced with latex irradiatedand latex not irradiated
(b) Shows the ratio between the size of micelles the Latex and silver NPs.

Fig. 3(a) shows a comparison of UV-visible spectra of silver nanoparticles produced in two different cases; the first case corresponds to latex/Ethanol solution which has been irradiated with microwave before its use in the synthesis of silver nanoparticles and the second one corresponds to the case where latex was not irradiated.

The irradiation of latex before adding Ag NO_3 precursor caused a red shift of the absorption peak, indicating that the size of silver nanoparticles became larger compared to the case where the latex was not irradiated. This behavior can be related to modification of the micelles properties, either their surface chemistry or surface roughness, or their size. Since the two samples were prepared by the same method, and same conditions we can conclude that there changes in surface properties and the increase in micelles size. The result suggested that the growth of silver nanoparticles was enhanced with the increase of the size of micelles.

Fig.3. (b) represents the ratio between the size of micelles the Latex and silver nanoparticles. This result indicated that the large size of micelles promote the increasing of silver nanoparticles size.

(a)   (b)
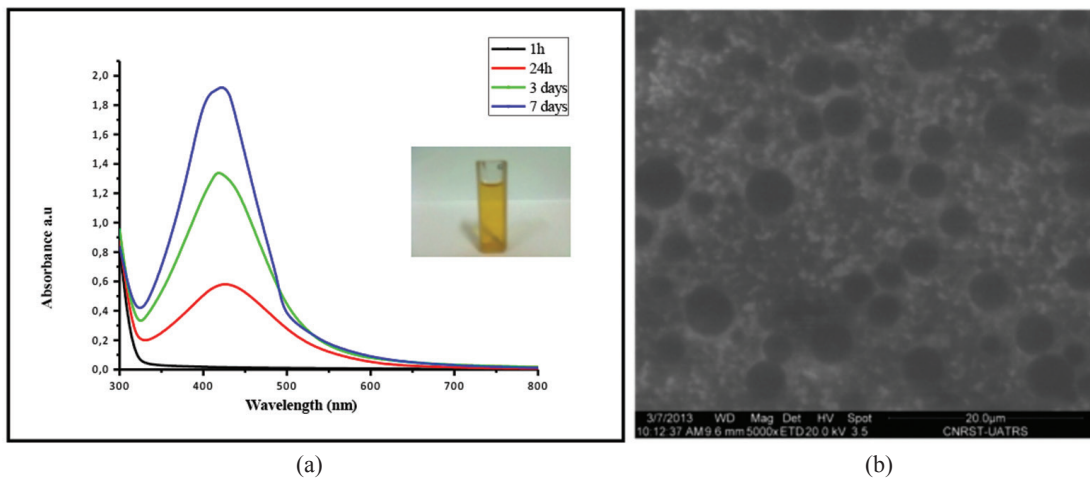
Fig. 4. (a) Absorption spectra of Ag NPs synthesis by self-assembly process
(b) SEM image of Ag NPs in the micelles of the latex.

Fig.4. (a) shows the UV-vis absorption spectra of silver nanoparticles after synthesis by self-assembly process at room temperature. The UV-vis spectra are characterized by the absorption maximum in the visible region at around 420 nm, which corresponds to the LSPR absorption region for silver nanoparticles spherical which is confirmed by scanning electron microscopy (SEM) in Fig. 4. (b). After 2 to 3 hours, the color of the solution became yellow, similar to the case of microwave method.

A   B

C

O = SURFACTANT MOLECULE
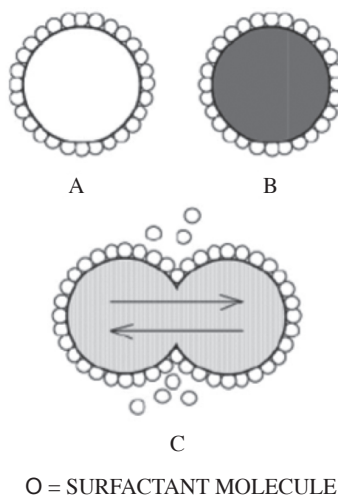
Fig. 5. The mechanism of silver nanoparticle fabricated by reverse micelle technique. [30]

Fig.5. Shows schematic of a collision between two reverse micelles. Collisions between micelles are frequent, and approximately one collision in every thousand results in the formation of a short-lived compound micelle. During the ~100 ns life time of the compound micelle, under micellar collision between droplets, it could offer enough energy to break the interfacial layer between micelles and penetrate each other. Two micelles would exchange the contents of their aqueous cores before separating, resulting in the eventual equilibrium distribution of all contents. Then, silver nanoparticles are synthesized from reactants solubilized in micelles. Resultant silver nanoparticles are coated by surfactants, and are dispersed in organic solvents, as shown in the TEM image of Fig. 6. (b) the encapsulating nanoparticles in micelles of Latex.

Functionalized surfactant could act as protective layer to prevent the oxidation of metal. Furthermore, nanoparticles fabricated by reverse micelle method are good candidates to self-assemble into novel nanostructures [26].

Emptied reverse micelles approach solid reactants again. Thus, the production of silver nanoparticles is promoted by repeating the process composed of the extraction of reactants, the synthesis of silver nanoparticles, and the dispersion of resultant silver nanoparticles. Last, the presence of the surfactant molecules in the micelles, which act as capping agents, may serve to prevent aggregation of the products.

Given the model of micelle interaction, the suitability of micelles as nanoreactors becomes evident. Since the size of the water pools in reverse micelles can be controlled by adjusting ωo and the Brownian motion of the particles allows the distribution of reactants, then not only reactions can be performed inside the micellar cores, but also the products would have nearly uniform size and shape.

Reverse micelles are generally characterized by ω_0, the molar ratio of water to surfactant (S):

$$\omega_o = [H_2O]/[S]$$

To establish the relationship between ω_0 and the micellar radius (R_M), it could; we can consider the micellar molar volume (V) given by

$$V_M = \frac{4\pi R_M^3}{3} = n_s V_s + n_W V_W$$

Where ns and n_w are the moles of surfactant and water per micelle, respectively, and V_w is the volume of water in the micelle. Assuming that the surface area of a micelle, Σ_M, is determined solely by the surfactant, then

$$\Sigma_M = 4\pi R_M^2 = n_s \Sigma_s$$

Where Σ_s is the molar interfacial area at the surfactant-oil boundary. Since the volume in this model is fixed, then

$$\omega_o = \frac{[H_2O]}{[S]} = \frac{n_W}{n_s}$$

$$R_M = \frac{3V_s}{\Sigma_s} + \frac{3V_W \omega_o}{\Sigma_s}$$

Some drops of the Ag–Latex solution were put on a glass substrate and dried at room temperature in air for some minutes. Subsequently, X-ray diffraction analysis was performed and the results are shown in Fig. 6. (a).

The XRD peaks at 2θ values of 8.38◦, 44.56◦, 64.82◦ and 77.77◦ can be attributed to the (111), (200), (220) and (311) crystallographic planes, respectively, of Bragg's reflections of the face-centered cubic (fcc) in structure of silver nanocrystals. The additional peak are observed at 2θ equal to about 32.6◦; they can be attributed to AgNO3 [29].

(a)   (b)
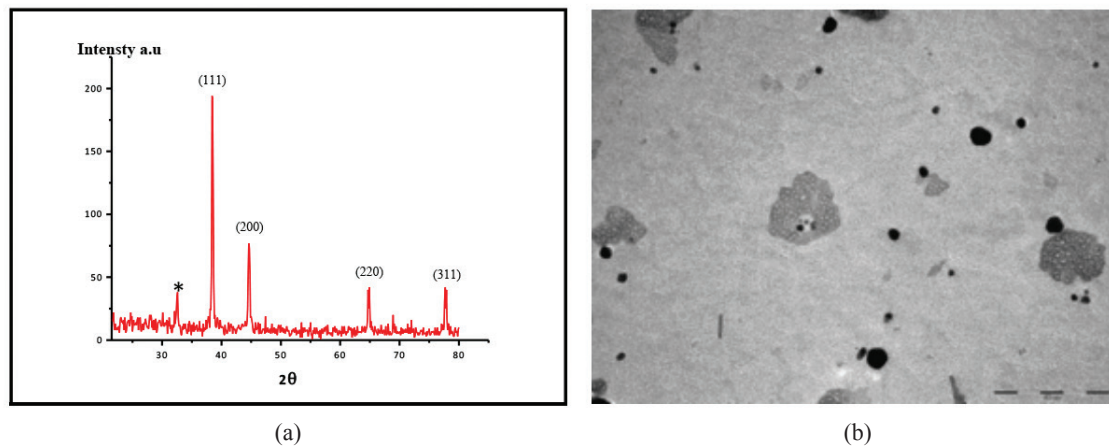
Fig. 6. (a) X-ray diffractogram in the Ag nanopowder.
(b) TEM image of Ag NPs the encapsulated in micelles of Latex.

(a)   (b)
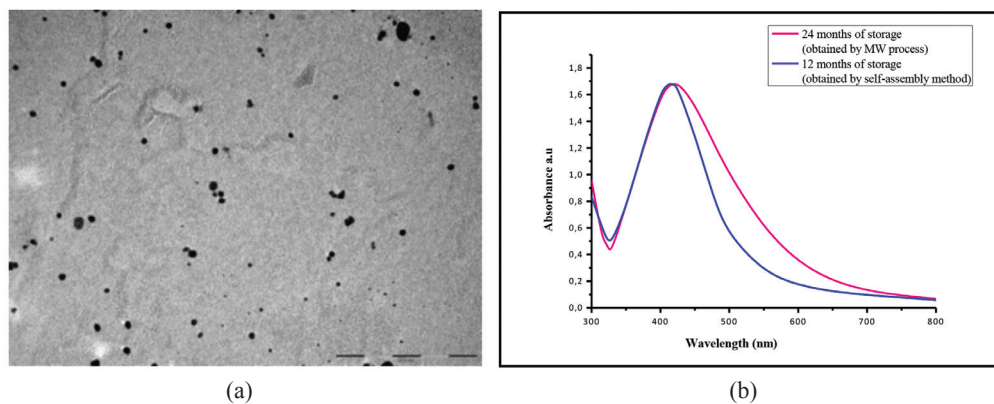
Fig. 7. (a) TEM image of Ag NPs synthesis by self-assembly method.
(b) UV-VIS of Ag-NPs after several months of storage

In both synthesis procedures, using microwave irradiation or by self-assembly process in reverse micelles, the obtained colloidal solutions with dispersed Ag NPs were highly stable and did not show any signs of visible change and aggregation, even after storage for several months at room temperature.

4. CONCLUSIONS

We have prepared Ag/Latex nanocomposites in Ethanol using simple solution chemistry by the two methods: microwave process and self-assembly. From the results obtained; we can estimate that all of the Ag-NPs the spherical shape of embedded Ag nanoparticles and their uniform with mean diameter 7 nm dispersion within the Latex matrix. The UV/vis spectra show the characteristic plasmon absorption peak for the Ag/Latex nanocomposites in the visible region for the EtOH at 415 nm.

The nanoparticles synthesized were found to be stable for several months, so they can be used for a long time after preparation. No other chemical is used either to facilitate the reaction or stabilize the metal in small particles.

Also, chemical reduction methods provide a direct means of up-scaling to meet mass manufacturing demands of nanoparticles.

We have demonstrated that the aggregation process of   silver nanoparticles   can be interpreted by a coalitional mechanism induced by the Brownian motion of copolymer micelles in the case of aggregation induced by a self-assembly process without need of Mw excitation.

References

[1]   T.J. Norman, C.D. Grant, D. Magana, J.Z. Zhang, J. Liu, D. Cao, F. Bridges, A.V.Buuren,J. Phys. Chem. B 106 (2002) 7005.

[2]   J.M. Wessels, H. Nothofer, W.E. Ford, F. Voneorochem, F. Scholtz, T. Vossmeyer, A.Schroedter, H. Weller, A. Yasuda, J. Am. Chem. Soc. 126 (2004) 3349.

[3]   Y. Wang, N. Toshima, J. Phys. Chem. 101 (1997) 5301.

[4]   G. Schmid, Chem. Rev. 92 (1992) 1709.

[5]   M.G. Bawendi, M.L. Steigerwald, L.E. Brus, Annu. Rev. Phys. Chem. 41 (1990)477;W.A. Deheer, Rev. Mod.Phys. 65 (1993) 611.

[6]   A.N. Shipway, M. Lahav, I. Willner, Adv. Mater. 12 (2000) 993.

[7]   H.Q. Jiang, S. Manolache, A.C. Wong, F.S. Denes, J. Appl. Polym. Sci. 93 (2004) 1411.

[8]   S. Hirano, Y. Vakasa, A. Saka, S. Yoshizawa, Y.O. Seimiya, Y. Hishinuma, A.Nishimura, A. Matsumoto, H. Kumakura, Phys. C 392 (2003) 458.

[9]   X.L. Ren and F.Q. Tang // Acta. Chim. Sinica. 60 (2002) 393.

[10] A. V. Kabanov ACS, Polymeric Materials Science and Engineering. Vol.76. Conference proceedings. San Francisco, Ca., Spring 1997, p.227. 01, 8.3 Biomedical Technology.

[11] N. Goetting, H Fritz, M Maier, J. Von Stamm, T. Schoofs; E. Bayer, Colloid & Polymer Science 277(2-3), 145 (1999).

[12] A. Pastou; H. Stamatis, A Xenakis, Progress in Colloid& Polymer Science 115, 192 (2000).

[13] M. Okubo, H. Ahmed, T. Suzuki, colloid & polymer 276(6), 470 (1998).

[14] D. A. Kaplan, C. D. Lytle, L. B. Routson, M. R. Myers, Alexandria,Thomas Jefferson Journal of Rubber Research 2(3), 3rd Quarter, 131 (1999).

[15] V. Aboutanos; L. A. P. Kane-Maguire; G. G. Wallace, Synthetic Metals 114(3), 313 (2000).

[16] F. M. Huijs, F. F. Vercauteren; B. de Ruiter,D. Kalicharan; G. Hadziioannou, Synthetic Metals102(1-3), 1151 (1999).

[17] S. Peper, I. Tsagkatakis, E. Bakker, AnalyticaChimicaActa 442(1), 25 (2001).

[18] O. Kalinina, E. Kumacheva, Macromolecules34(18), 6380 (2001).

[19] Advanced Materials 13(4), 286 (2001).

[20] Y. G. Durant, D. C. Sundberg, Macromolecules29(26), 8466 (1996).

[21] J. F. Anstey; N. Subramaniam; B. T. T. Pham; X. Lu; M. J. Monteiro; R. G. Gilbert, Macromolecular Symposia 150, 73 (2000).

[22] Z. Z. Yang; Y. Z. Xu; D. L. Zhao; M. Xu, Colloid&Polymer Science 278(11), 1103 (2000).

[23] M. Zubitur; J. M. Asau, Polymer 42(14), 5979 (2001).

[24] L. Fu-Ken, H. Pei-Wen, C. Yu-Cheng, K. Chu-Jung, K. Fu-Hsiang, C. Tieh, J. Cryst. Growth 273 (2005) 439.

[25] A. Heilman, Polymer Films with Embedded Metal Nanoparticles, Springer-Verlag, Berlin, Heidelberg, 2003.

[26] Taleb, A.; Petit, C.; Pileni, M. P. Chem. Mater. 1997, 9, 950

[27] (a) Liveri, V. T. Controlled Synthesis of Nanoparticles in MicroheterogeneousSystems, Springer; New York, 2006. (b) Liz-Marzán L. M.; Kamat, P. V. Nanoscale Materials, Kluwer Academic Publishers; Boston, 2003.

[28] Cushing, B. L.; Kolesnichenko, V. L.; O'Connor, C. J. Chem. Rev. 2004, 104, 3893.

[29] S. Clemenson, L.David, E. Espuche, Structure and morphology of nanocomposite films prepared from polyvinyl alcohol and silver nitrate: influence of thermal treatment, J. Polym. Sci. Part A: Polym. Chem. 45 (2007) 2657–2672.

[30] Cushing, B. L.; Kolesnichenko, V. L.; O'Connor, C. J. Chem. Rev. 2004, 104, 3893.

Pulsed thermography model for detecting the internal ferritic steel crack

A. Elhassnaoui[1,2], S. Yadir[1], A. Saifi[1], A. Elamiri[1], S. Sahnoun[1,*]

[1] Laboratory of Electronics, Instrumentation and Energetic, Faculty of Sciences,
B.P 20. 24040 - El Jadida, Morocco.

[2] Laboratoire de Génie Industriel, Faculté des Sciences et Techniques B.P : 523 Béni Mellal

* Corresponding author: ssahnoun@gmail.com

Abstract. *The cracks in steel parts may occur near the contact surfaces under the effect of concomitant constraints. The growth mechanisms crack and its emergence are not currently known with certainty. With the finite element method we have developed a mathematical model to determine the crack depth from the standard thermal contrast taking into account of the contrast time values. We found that the flux density and pulse duration have no remarkable influence on the thermal image samples. We calculated the proposed model accuracy, and the optimal value of the theoretical measurement time.*

The simulation results show that pulsed thermography is adapted to inspection and characterization the internal cracks into steel.

Keywords: characterization, finite element method, Pulsed thermography Non destructive testing, cracks into steel.

1- Introduction

Defects are any deviation from the reference. For steel parts, most frequently apear during the manufacturing phase. Manufacturing defects weakening the parts and reduces their hard service. Therefore, the developments of inspection methods to evaluate the presence of cracks in steel parts and measure its depth are considerably interesting.

The pulsed thermography (PT) is a method of non-destructive evaluation that has been applied in the inspection of different materials for detecting the presence of defects [1-8]. For many applications, pulsed thermography (PT) compares favorably to conventional inspection technologies in terms of its sensitivity and speed, while offering some advantages in terms of curvature tolerance and non-contact inspection [9]. Its quantitative characterization to extract defect depth, size and thermal properties has been proven effective [10-12].

Using a 3D finite element simulation, we are going to highlight in the first part of this work the ability of pulsed thermography (PT) in detecting inner cracks steel. In the second part we show the effects of the heat flux density, the pulse duration and the defect depth on the standard thermal contrast in order to determine the values which can gives the best results.

In the third part, we propose a model for estimating the crack defect depth from standard thermal contrast; after having defined the best conditions for the PT method application.

2- Model description

Pulsed thermography (PT) is a technique widely used in active thermography approaches. It is characterized by its speed and ease of implementation. To study the ability of pulsed thermography (PT) in the detection of crack defects on steel .parts; we simulate the detection process by the 3D finite element method, for that, we consider isotropic steel samples with square shape and edge equals to 10cm. The sample contains a round flat bottom hole with diameter equal to 20 mm and located at depths ranging from 0.5 to 6 mm (Figure 1).

The thermal properties of the used material are as follows:

- The specific heat: 490 J/kg.K,

- The thermal conductivity: 47.5 W/m.K,

- The density: 7870 kg/m^3.
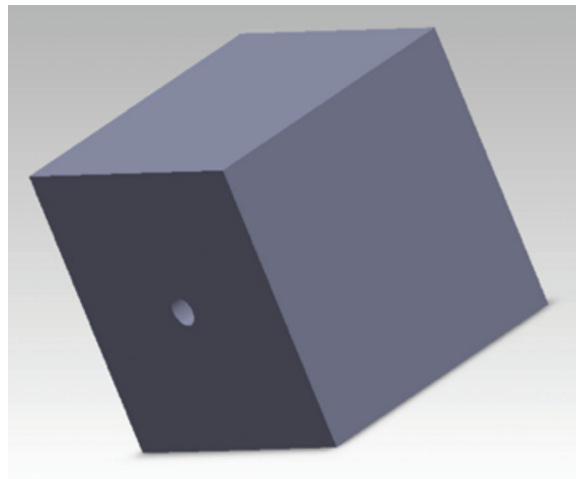
Figure.1: 3D round bottom hole model

In pulsed thermography method, the detection and characterization of a defect is based on the relative thermal contrast C(t) between suspicious area and unflawed area. We apply a heat flux of short duration on the surface above the defect and we calculate, the surface temperature distribution as a function of time by a software based on finite element method,.

We define the standard thermal contrast C(t) by the difference between values of the surface temperature over flawed zone and over the flawless zone by [12]:

$$C(t) = \frac{T_{def}(t) - T_{def}(t_0)}{T_s(t) - T_s(t_0)}$$

(1)

Where:

- Tdef(t): the surface temperature above the flawed zone at the time t,

- Tdef(t0): the surface temperature above the flawed zone just before pulse heating,

- Ts(t): the surface temperature over the unflawed zone at the time t,

- Ts(t0): the surface temperature over the unflawed zone just before pulse heating.

3- Effect of crack depth on the variation of standard thermal contrast

The pulse duration is important in detecting crack defect. Figures 2-a, 2-b and 2-c show the variations of the standard thermal contrast as a function of time in the case where flux density is equal to 3000 W/m² during Δtp =5ms, 10ms and 15ms.
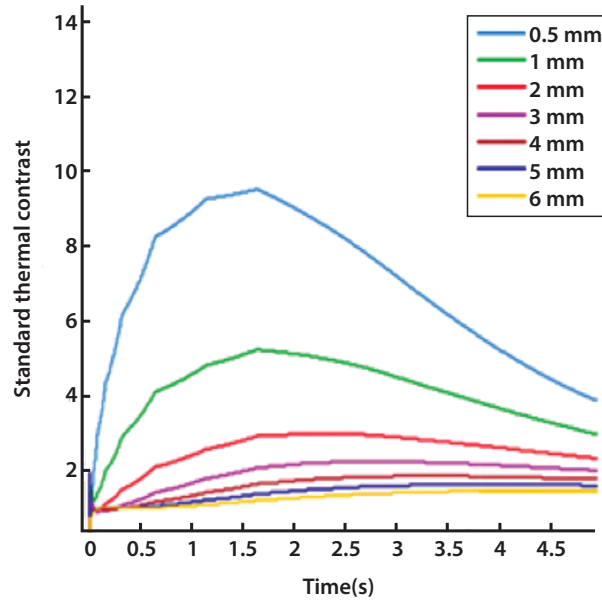
Figure.2-a standard thermal variation contrast versus time, pulse duration Δtp = 5ms
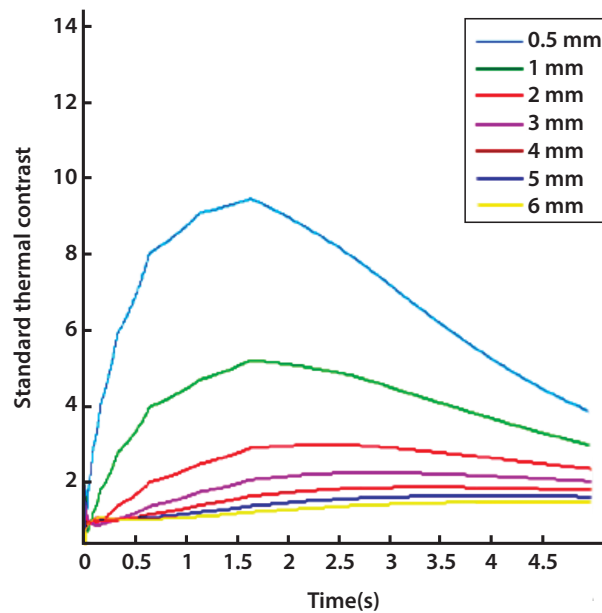
Figure.2-b standard thermal variation contrast versus time, pulse duration Δtp = 10ms
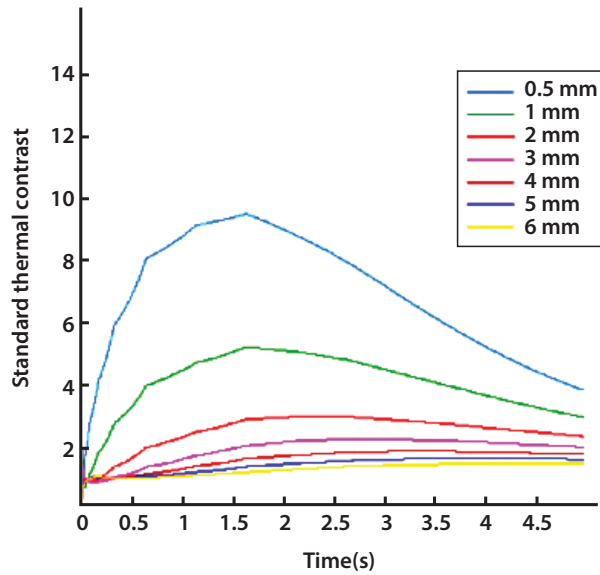
Figure.2-c Variation of standard thermal contrast versus time, pulse duration Δtp = 15ms

We can note that in the studied configuration, the defect depth is influential on standard thermal contrast. We find that the near-surface defects have important values of standard thermal contrast. In case where defects are far from the surface (0.5mm <z <6mm), standard thermal contrast curves are superimposed and become difficult to distinguish. The theoretical measurement time tm is an important parameter in the PT method. The choice of this moment is crucial, in this time tm we must be able to differentiate between the thermal contrast of each depth, we propose in this case to choose a value tm between 1.25s and 2.5s; because in this interval the standard thermal contrast is maximum for most of defects depth.

4- Effect of the intensity of the flux density on the detection of crack defects on steels parts

To study the effect of the intensity of the flux density on the steel crack detection by PT method, we considered three different pulse durations Δtp, 5ms, 10ms and 15ms. For each pulse duration, we varied the intensity of the flux density, applied on the sample surface, between 1000 W/m^2 and 6000 W/m^2. In Figures 3-a, 3-b and 3-c, we have shown variation of standard thermal contrast versus defect depth, the theoretical measurement time is tm=2s.
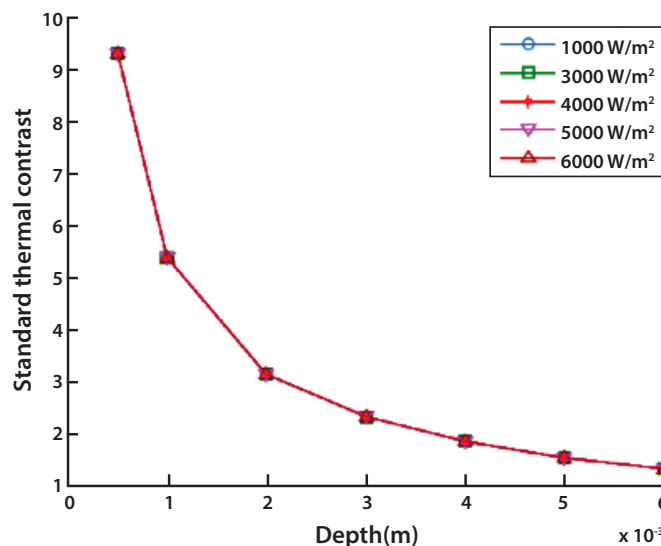
Figure.3-a Standard thermal contrast variation versus defect depth,pulse duration Δtp = 5ms
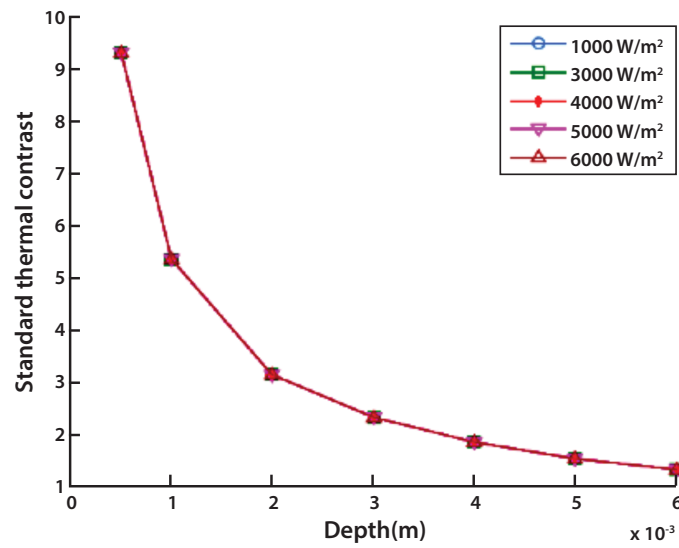
Figure. 3-b Standard thermal contrast variation versus defect depth, pulse duration Δtp =10ms
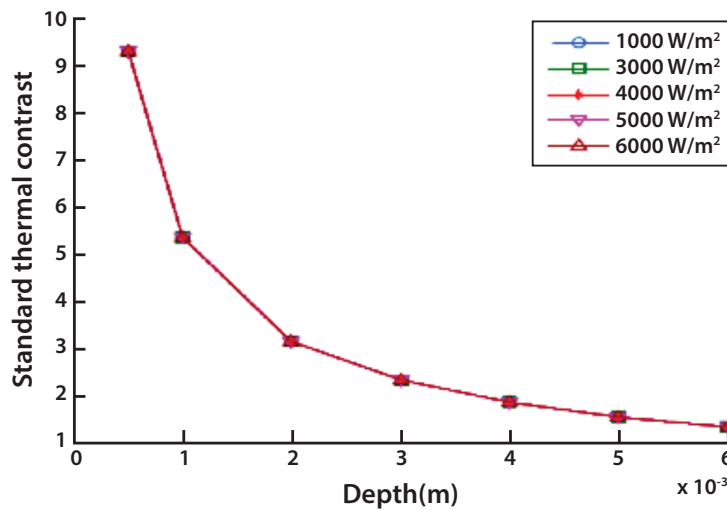
Figure. 3-c Standard thermal contrast variation versus defect depth, pulse duration Δtp =15ms

We note that for all pulse duration, the curves are superimposed. Therefore, the change in flux density has no remarkable influence on the standard thermal contrast whatever the defect depth.

5- Effect of pulse duration on the crack defect detection

To study the effect of the pulse duration, we set the flux density at 6000 W/m², and we have plotted in Figure 4 below the variation of standard thermal contrast, taken at the theoretical measurement time tm = 2s, as a function of the defect depth. The considered pulse durations Δtp are 5ms, 10ms and 15ms.

Frontiers in Science and Engineering - Vol. 5 - n°2 - 2015
An International Journal Edited by The Hassan II Academy of Science and Technology

35
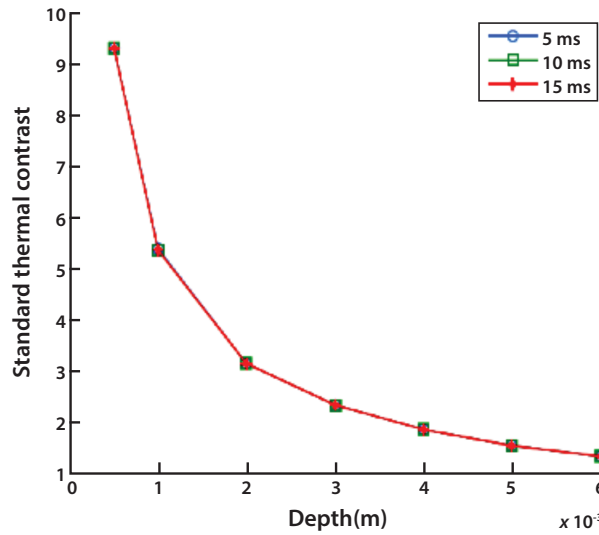
Figure.4: Standard thermal contrast variation versus defect depth, flux density = 6000 W/m^2

We note that the pulse duration has no effect on the standard thermal contrast values; indeed the curves in Figure 4 are superimposed and the response of the material is the same whatever the pulse duration.

One of objectives of railway infrastructure operators is to make a more effective and less costly preventive maintenance of the railway network. So they seek inspection tools and defect characterization, simulation tools for detecting defects and predicting their evolution enabling better prevention of ruptures frequently encountered on the rails.

6- Model to estimate the crack defect depth from standard thermal contrast

After a preliminary study on the effects of selected major parameters in the development of instrumentation for NDT steel inspection. To develop simulation tools to predict the presence and evolution of defects, we propose in this section a law to estimate the defect depth from the standard thermal contrast; we performed simulations with fixing the flux density at 6000 W/m2 and the pulse duration to 15ms. We have plotted in Figure 5 crack defect depth variation as a function of standard thermal contrast for three theoretical measurement time tm 1.5s, 2s and 2.5s.
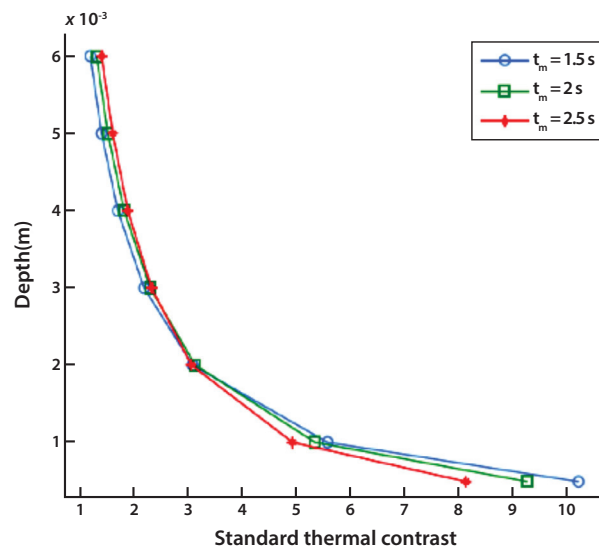
Figure.5: Defect depth variation versus standard thermal contrast, pulse duration Dtp=15ms, flux density = 6000 W/m^2

We note that the shallow depths provide important contrasts, however great depths have the same contrast. The defect depth is slightly sensitive to the choice of the theoretical measurement time tm. For the theoretical measurement time tm value between 1.25s and 2.5s, we propose one model that allows estimating the defect depth from the thermal contrast in PT method.

The model is as follows:

$$p(c, t_m) = A(t_m).[Exp[\frac{B(t_m)}{c}] - 1]$$

Where:

p(c,tm): the estimated value of the defect depth,

c: the standard thermal contrast value,

tm: the theoretical measurement time of standard thermal contrast c.

The coefficients A(tm) and B(tm) are given by:

$$A(t_m) = 0.00183724t_m^2 - 0.0124421t_m + 0.0229113 \qquad (3)$$

$$B(t_m) = 0.209987t_m^2 - 0.027009t_m + 0.235193 \qquad (4)$$
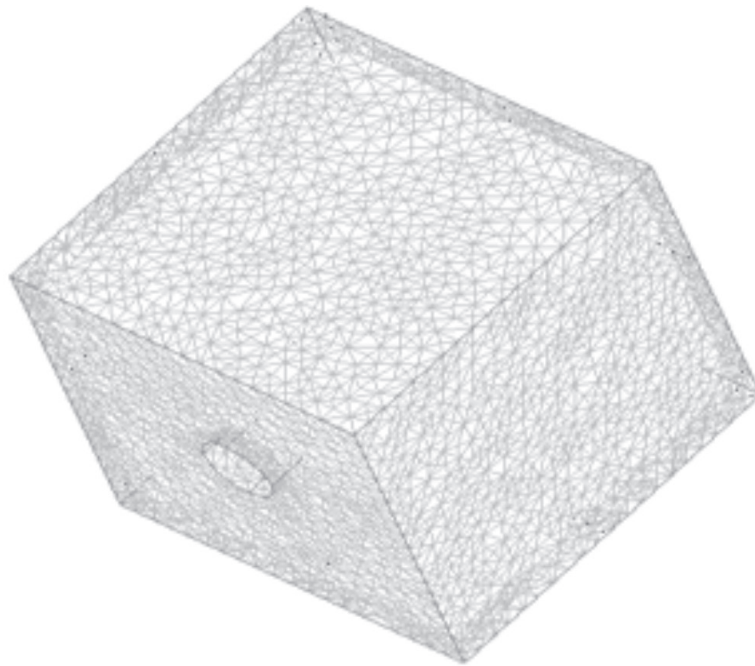
Figure.6: 3D model by finite element

To verify the model and as we do not currently have measurement means, so we simulated by 3D finite elements a piece of steel that contains a defect crack located at different depths Figure 6. In Figures 7-a, 7-b, 7-c, 7-d, 7-e and7-f, we superimposed the results obtained by simulation and the results obtained by the proposed model in the relationship (2). We plotted the variations of the defect depth as a function of standard thermal contrast for different measurement times.
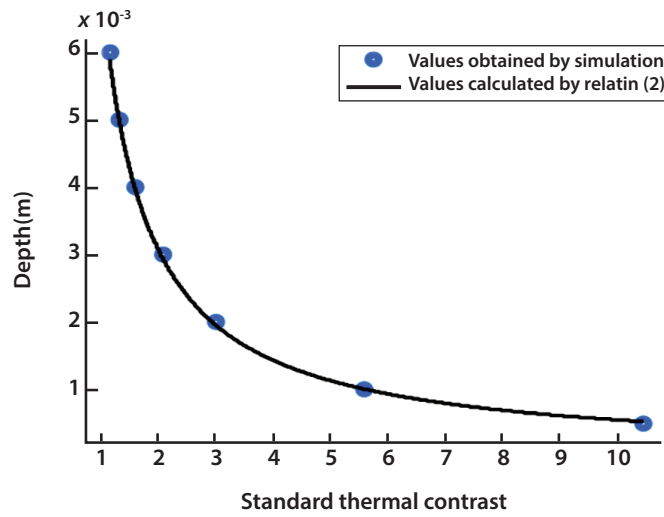
Figure.7-a Proposed model results for time tm=1.25s.
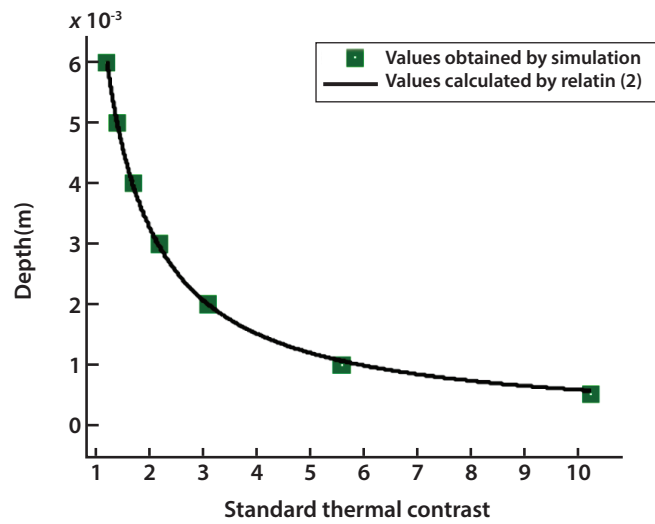
Figure.7-b Proposed model results for measuring time tm=1.5s.
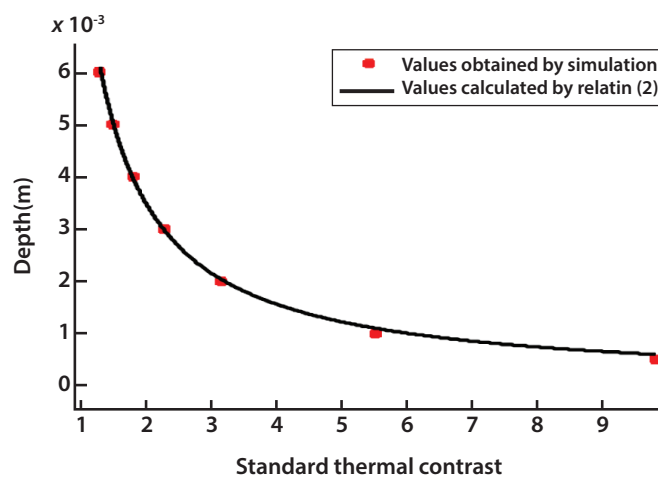
Figure.7-c Proposed model results for the theoretical measuring time tm=1.75s.
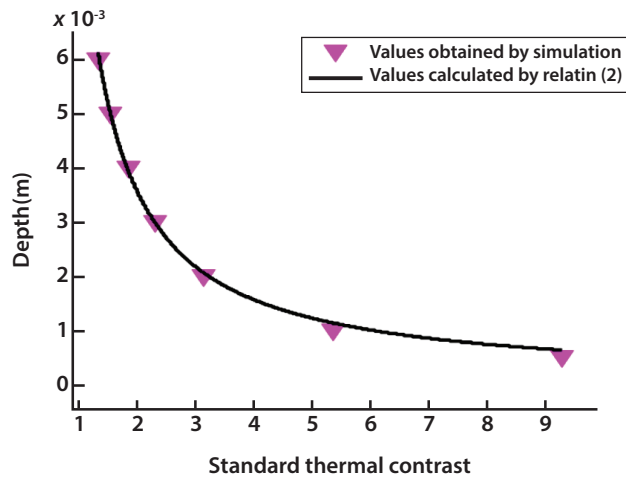
Figure.7-d Proposed model results for the theoretical measuring time tm=2s.
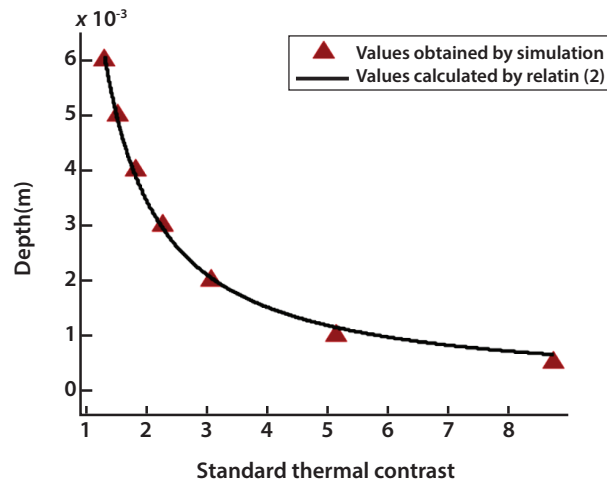
Figure.7-e Results of the proposed model for measuring time tm=2.25s.
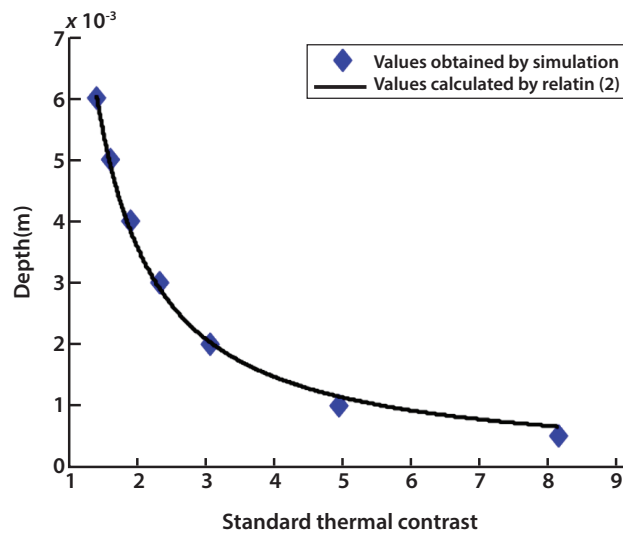
Figure.7-f Results of the proposed model for measuring time tm=2.5s.

To evaluate the precision of the model results, we defined the difference between the model estimation and simulation by the following arithmetic average:

$$error = \frac{\sum_{i=1}^{n} \left| p_{real}^i - p_c^i \right|}{n} \tag{5}$$

Where

- p_{real}^i is the actual depth corresponding to the ith point obtained by simulation,

- p_c^i is the calculated depth by the proposed model relationship (2),

- n is considered points number.

The obtained error values remain low for most measurement times. The optimal value that allows having the minimum difference (error) is tm = 1.5s. See table 1 where we reported the gap between the two values:

Measurement time	tm=1.25s	tm=1.5s	tm=1.75s	tm=2s	tm=2.25s	tm=2.5s
(Error (mm	10-2 4.5843	10-2 3.8697	10-2 6.3957	10-2 7.3404	10-2 8.7429	1.027710-1

Table 1: gap between the values

The proposed model is used to estimate the defect depth inner steels crack from standard thermal contrast that can be provided by the infrared camera taking into account the theoretical measurement time tm.

7- Conclusion

In this article, we showed the ability of the method of pulsed thermography to detect internal cracks steels like steels parts used in thermal power plants to produce electricity. This tool allows us to propose the steels best suited to specific situations. These bases will be used to supply simulation tools and calibrate the new parts model.

We found that in crack defects inspection by pulsed thermography, the flux density and pulse duration have no remarkable influence on the thermal image samples. Instead, the standard thermal contrast depends on the cracks depth. In the end, by the finite element method we have proposed a mathematical model to determine the crack depth from the standard thermal contrast taking into account of the contrast time values. We calculated the overall accuracy of the proposed model, and we found that the optimal value of the theoretical measurement time is about 1.5s.

References

[1]   M. Kerr, A. Wilson, S. Marich, Rail-the-core of integrated transport, in: Proceedings of CORE 2008 Conference on Railway engineering: RTSA, Engineers Australasia, Perth, Australia, 2008, p. 83.

[2]   S. Marich, S. Mackie, The development of squat defects under high axle load operations, in: Proceedings of CORE 2002 Conference on Railway engineering: RTSA, Engineers Australasia, Wollongong, Australia, 2002, p. 17.

[3]   X. Maldague, Nondestructive Evaluation of Materials by Infrared Thermography, Springer, New York, 1993.

[4]   Steven M. Shepard, Flash thermography of aerospace composites, in: IV Conferencia Panamericana de END Buenos Aires, Octubre 2007.

[5]   A. Elhassnaoui, A. Elballouti, S. Sahnoun, Reconstruction of a triangular geometry defects in inaccessible face by a model of active thermography, J. Optoelectron. Adv. Mater. 15, 5-6, (2013) 447.

[6]   A. Elhassnaoui, A. Saifi, A. Elamiri, S. Sahnoun, A simple method for determining the thermal effusivity of defects, Eur. Phys. J. Appl. Phys. 66 (2014) 20501.

[7]   A. Elhassnaoui, S. Sahnoun, A three-dimensional reconstruction algorithm for pulsed thermography, J. Mater. Environ. Sci. 5 (4) (2014) 983-988.

[8]   A. Elhassnaoui, A. Saifi, A. Elamiri, S. Sahnoun, Modeling of the lock-in thermography process through finite element method for measuring of the thermal diffusivity, International Journal of Innovation and Applied Studies, 5 (4) (2014) 354-359.

[9]   D.P. Almond, S.K. Lau, Defect sizing by transient thermography I. An analytical treatment, J. Phys. D Appl. Phys. 27 (5) (1994) 1063–1069.

[10] D.W. Tang, G.H. He, B.L. Zhou, Effects of finite absorption depth and infrared detector non-linearity on thermal diffusivity measurement of thin films using the flash method, Rev. Sci. Instrum. 66 (1995) 4249–4253.

[11] J.G. Sun, Analysis of pulsed thermography methods for defect depth prediction, J. Heat Transfer 128 (4) (2006) 329.

[12] X.P.V. Maldague, Theory and Practice of Infrared Technology for Nondestructive Testing, Willey-Interscience, New York, 2001, pp. 198–199.

Global solar radiation estimation on a horizontal and a tilted plane in Agadir city, Morocco

M. Elyaqouti[1], L. Bouhouch[2] & A. Ihlal[3]

[1,2] ERTIAER, EST Agadir, Ibn Zohr University, Agadir, Morroco

[3] LMER, FS Agadir, BP 8106, Ibn Zohr University, Agadir, Morroco

[1] elyaqouti@gmail.com, [2] l.bouhouch@uiz.ac.ma, [3] a.ihlal@uiz.ac.ma

Abstract. *In this paper, we propose the modeling and simulation of the incident solar radiation on a horizontal and an inclined plane in the city of Agadir. For this concern, we adopt the clear sky model proposed by Kasten, which takes into account some aspects of the atmospheric turbidity into consideration in order to estimate the incidental solar radiation on a horizontal plane. In addition we determine the incident solar radiation on an inclined plane from the global horizontal radiation. To validate the chosen model, we compare the simulated values of the solar radiation with the experimental measurements given by our CRX10 Campbell meteorological station installed in the location of this study..*

Keywords: Prediction; Solar radiation; Kasten model; Klucher model.

1. Introduction

Renewable energy resources have huge potential and can satisfy the present and future energy demand. These resources can enhance diversity in energy supply markets, secure long-term sustainable energy supply, and reduce local and global atmospheric emissions [1]. When we consider solar energy resources, an estimation of the amount of incident solar radiation on an area is usually required for many solar energy applications. Therefore, several radiation models have been proposed [2].

In this paper, we propose the modeling and simulation of the incident solar radiation on a horizontal and an inclined plane in the city of Agadir.

2. Meteorological data

Meteorological data, such as irradiation data and temperature are delivered from the data logger CRX10X installed at EST of Agadir (Fig. 1). This station is equipped with various sensors for the acquisition of global and diffuse irradiation, the ambient temperature, humidity, speed and wind direction. The measured values can be presented in different forms (average, maximum, minimum…), depending on the chosen configuration. The used data in this work are related to the site of Agadir, whose geographical coordinates are: $\phi = 9.579$ °W for the longitude, $L = 30.406$ °N for the latitude and $Z = 41$ m for the altitude.

Fig. 1. Meteorological station with the data logger Campbell CR10X

3. Modeling

3.1 Sun declination

The sun declination δ is the angle between the rays of the sun and the plane of the earth's equator. It's expressed as a function of day number *n* by the following formula [3]:

$$\delta = 23.45 \sin\left[360*(284+n)/365.25\right] \qquad (1)$$

3.2 Hour angle

The hour angle *H* is the solar angular displacement east or west of the local meridian due to the rotation of the earth (15° per hour). The hour angle is negative in the morning and positive in the afternoon. Therefore, the hour angle can be written as follows [1]:

$$H = 15°(RTS - 12) \qquad (2)$$

Where *RTS* is real time solar (in hours). It is counted from 0 to 24 h. It is calculated by the following relationship:

$$RTS = T_{legal} + ET - \frac{L - L_{ref}}{15} - C \qquad (3)$$

Where T_{legal} is the legal time, *C* is the time difference between the legal time and civil time of the location, $L\text{-}L_{ref}$ is the difference in longitude between the place and the considered as the reference time legal and *ET* is the correction of the time equation, due to the variation of the earth speed on its path around the sun. It can be calculated by the following expression:

$$ET = -0.0002 + 0.47497\cos(x) - 7.3509\sin(x) - 3.2265\cos(2x) - 9.3912\sin(2x) - 0.0903\cos(3x) - 0.3361\sin(3x)$$
$$(4)$$

Where:

$$x = 360n/366 \qquad (5)$$

3.3 Solar coordinates (zenithal and azimuth angles, altitude)

The zenith angle θ_z is defined as the angle between the vertical and the line to the sun, which is the angle of incidence of a beam radiation on a horizontal plan, it's can be calculated as [1]:

$$\cos(\theta_z) = \cos(\delta)\cos(\varphi)\cos(h) + \sin(\varphi)\sin(\delta) \qquad (6)$$

The solar altitude angle *h* is the angle between the horizontal and the line to the sun that is the complement of the zenith angle. It can be expressed using the following equation:

$$\sin(h) = \cos(\delta)\cos(\varphi)\cos(H) + \sin(\varphi)\sin(\delta) \qquad (7)$$

The solar azimuth angle a_s is defined as the angular displacement from south of the projection of beam radiation on horizontal plan [1]. It can be calculated as:

$$\begin{aligned} a_s &= \arcsin\left(\cos(\delta)\sin(H)/\cos(h)\right) & si \quad \cos(h) \geq \tan(\delta)\tan(L) \\ a_s &= 180 - \arcsin\left(\cos(\delta)\sin(H)/\cos(h)\right) & si \quad \cos(h) \, \text{p} \, \tan(\delta)\tan(L) \end{aligned} \qquad (8)$$

3.4 Incidence angle

The incidence angle θ_i is the angle between the beam radiation and the normal to the surface with any orientation. It can be expressed using the following equation:

$$
\begin{aligned}
\cos(\theta_i) \ = \ & \sin(\delta)\sin(\varphi)\cos(\beta) - \sin(\delta)\cos(\varphi)\sin(\beta)\cos(a_p) + \cos(\delta)\cos(\varphi)\cos(\beta)\cos(H) \\
& + \cos(\delta)\sin(\varphi)\sin(\beta)\cos(a_p)\cos(H) + \cos(\delta)\sin(\beta)\sin(a_p)\sin(H)
\end{aligned}
\tag{9}
$$

Where a_p is the surface azimuth which is the deviation of the projection on a horizontal plane of the normal to the surface from the local meridian, β referred also the surface inclination.

3.5 Global radiation modeling on a horizontal plane

In order to estimate the incident solar radiation on a horizontal plane, we used the Kasten model [8][4]. It's a model that takes the atmospheric turbidity into consideration.

The global radiation G on a horizontal plane is the sum of diffuse radiation G_{diff} and the direct radiation G_{dir}. It is expressed as follows:

$$
G = G_{dir} + G_{diff}
\tag{10}
$$

The beam radiation G_{dir} is defined as solar radiation that travels from the sun to the earth's surface without any scattering by the atmosphere [1]. It can be expressed using the formula of Kasten as follows:

$$
G_{dir} = \left(I_0\right)_{ext} \exp\left[-\frac{m_h T_L}{0.9 m_h + 9.4}\right] \sin(h)
\tag{11}
$$

Where $(I_0)_{ext}$ is the average incident radiation on a plane perpendicular to the rays at the upper limit of the atmosphere, it's equal to $(I_0)_{ext}$=1366 W.m^{-2}, and m_h is the atmospheric optical distance, called air mass (m). It can be written as follows:

$$
m_h = \frac{1 - 0.1Z}{\sin(h) + 0.15\left(h + 3.885\right)^{-1.253}}
\tag{12}
$$

T_L is the Linke turbidity factor. It gives an evaluation of the atmospheric extinction by gaseous molecules and aerosols. Its average value is given by the following expression [5]:

$$
T_L = 2.5 + 16\beta_A + 0.5\ln(w)
\tag{13}
$$

β_A is the Angstrom coefficient and w is the height of condensable water ($\beta_A = 0.05$ and $w = 1$ cm for a clear sky).

The diffuse radiation G_{diff} is solar reaching the earth's surface after having been scattered from the direct solar beam by molecules in the atmosphere. It can be expressed using the following equation:

$$
G_{diff} = \frac{\left(I_0\right)_{ext}}{25} \sqrt{\sin(h)} \left[T_L - 0.5 - \sqrt{\sin(h)}\right]
\tag{14}
$$

3.6 Global radiation modeling on tilted planes

The global radiation on a tilted surface G_β is the sum of the diffuse radiation $G_{diff,\beta}$, beam radiation $G_{dir,\beta}$, and the ground reflected radiation $G_{ref,\beta}$. Therefore, the incident global radiation on tilted surface is given by the following expression [4]:

$$G_\beta = G_{dir,\beta} + G_{ref,\beta} + G_{diff,\beta} \tag{15}$$

The beam radiation on tilted surface $G_{dir,\beta}$ can be estimated by multiplying its value on a horizontal surface G_{dir} by a geometric factor R_b which depends on the zenith and incidence angles. It's expressed as:

$$G_{dir,\beta} = G_{dir} R_b = G_{dir} \frac{\cos(\theta_i)}{\cos(\theta_z)} \tag{16}$$

The ground reflected radiation is assumed as follows [6]:

$$G_{ref,\beta} = \frac{1}{2} \rho G \left(1 - \cos\beta\right) \tag{17}$$

According to the Klucher model [7], the diffuse solar radiation on tilted planes can be given by the following expression:

$$G_{diff,\beta} = G_{dir} \left[0.5\left(1 + \cos(\frac{\beta}{2})\right)\right]\left[1 + \left(1 - \left(\frac{G_{diff}}{G}\right)^2\right)\sin^3(\frac{\beta}{2})\right]\left[1 + \cos^2(\theta_i)\sin^3(\theta_z)\right] \tag{18}$$

4. Results and discussions

At first let's bear in mind that several models are used to estimate the solar radiation falling on earth. In this study we have chosen the Kasten model because of its simplicity compared to other complex models [8]. We have considered a sample of recorded measurements by the installed meteorological station in the location of the present study. The measured data cover a long period from 2009 to 2013.

Figures 1 and 2 provide a comparison between this solar radiation with that delivered by our model developed under Matlab for the days of July 1st 2011 and March 12th 2012.

In order to judge the reliability of the proposed model at our site and to determine the error of the incident radiation, we calculate the committed instantaneous relative error using the equation (19):
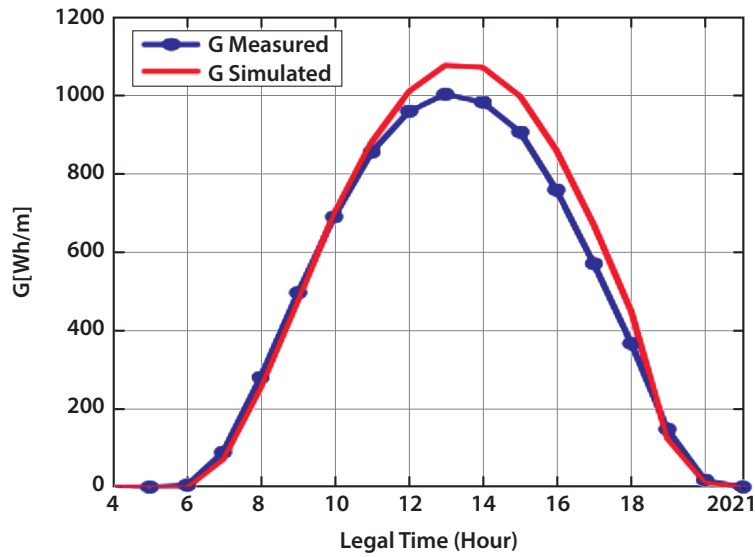
Fig. 2. Global solar radiation on a horizontal surface for July 1st 2011
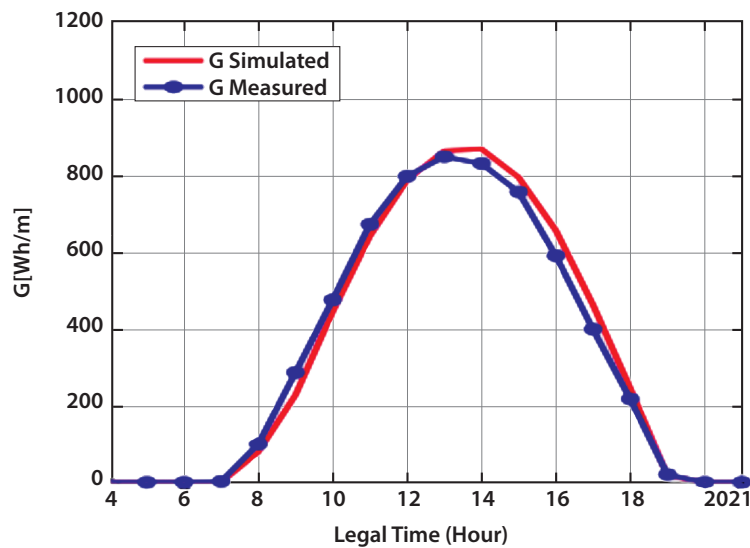
Fig. 3. Global solar radiation on a horizontal surface for March 12th 2012

$$Err = \frac{G_{measured} - G_{calculated}}{G_{measured}} \qquad (19)$$

The values of this error for both days of the selected sample are shown in Figure 3. These values show that the instantaneous relative error does not exceed 10% between 10 AM and 15 PM, with a maximum value of -22% for the day of March 12th 2012 at 18 PM. This shows that our model gives satisfactory results, allowing its validity. For inclined surfaces of an angle β = 15, 30, 45 and 60 °, we represent in Figure 4 the received global solar irradiance G on these surfaces. We notice an increase in received solar radiation by surfaces inclined relative to horizontal surfaces. Our simulation shows that the solar irradiance is proportional to the angle of inclination.
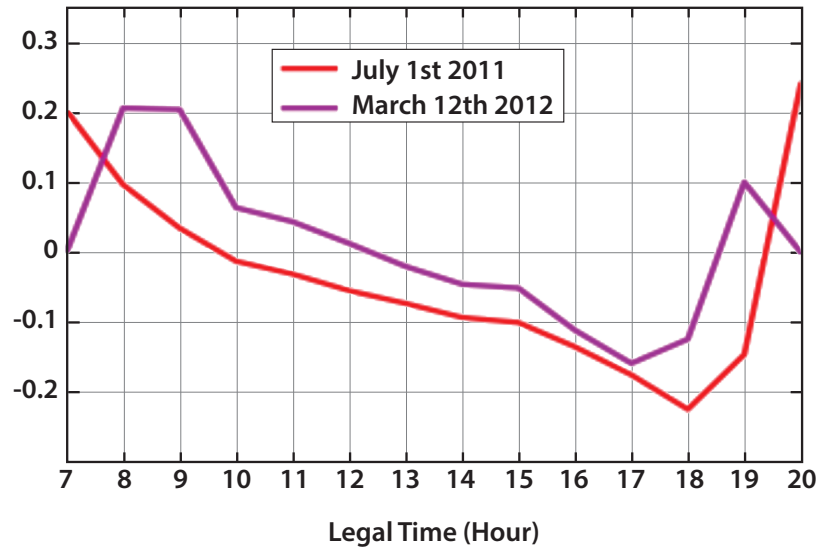
Fig. 4. Relative error of the global solar radiation on a horizontal surface for both selected days
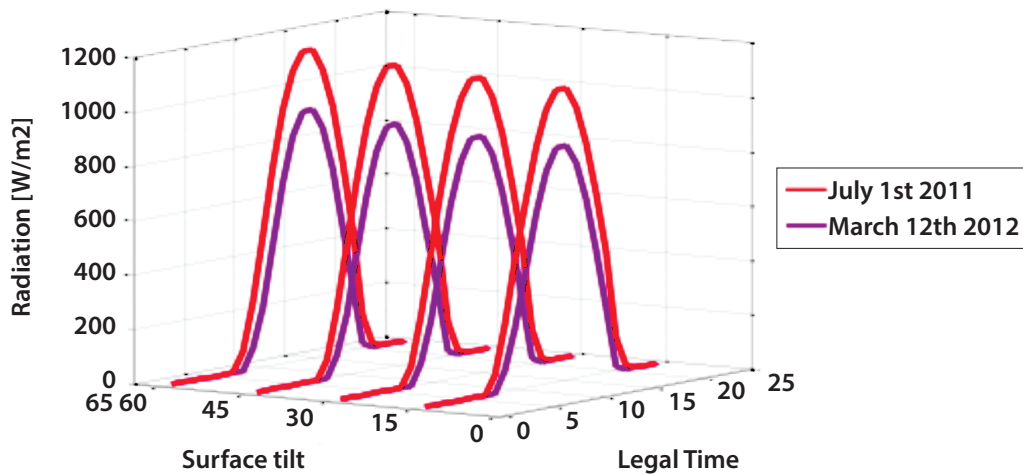
Fig. 5. Global solar radiation for different angles and for both selected day

5. Conclusion

In this work, we present the estimation of solar radiation on a horizontal plane as well as on an inclined one using a Kasten model. The measurements collected by the meteorological station installed in our laboratory have allowed validating the chosen model for the prediction and estimation of incident solar radiation on horizontal surfaces. According to simulations, the proposed model, validated by measures, provides that solar irradiance is proportional to inclination angle.

References

[1] T. Maatallah, S. El Alimi, S. Ben Nassrallah, Performance modeling and investigation of fixed, single and dual-axis tracking photovoltaic panel in Monastir city, Tunisia, Renewable and Sustainable Energy Reviews, Vol. 15, Issue 8, (2011), pp. 4053-4066.

[2] S. Janjai, K. Sricharoen, S. Pattarapanitchai, Semi-empirical models for the estimation of clear sky solar global and direct normal irradiances in the tropics, Applied Energy, Vol. 88, Issue 12, (2011), pp. 47494755.

[3] R. Pon Vengatesh, S. Edward Rajan, Investigation of cloudless radiation with PV module employing Matlab-Simulink, Solar Energy, Vol. 85, Issue 9, (2011), pp. 1727-1734.

[4] B. Ould Bilal, V. Sambou, C.M.F. Kebe, M. Ndongo, P.A Ndiaye, Etude et modélisation du potentiel du site de Nouakchott et de Dakar, Journal des Sciences, Vol. 7, N°4, (2007), pp. 5766.

[5] Mohamed Ansoumane Camara, Modélisation du stockage de l'énergie photovoltaïque par super-condensateurs, Thèse de Doctorat, Université Paris-Est Creteil, (2011).

[6] R Posadillo, L.R. López, Evaluation of the performance of three diffuse hourly irradiation models on tilted surfaces according to the utilizability concept. Energy Conversion and Management, Vol. 50, Elsevier 09, (2009), pp. 2324-2330.

[7] T.M. Klucher, Evaluation of models to predict insolation on tilted surfaces, Solar Energy, Vol. 23, Issue 2, (1979), pp. 111-114.

[8] P.H. Communay, Héliothermique: le gisement solaire, méthodes et calculs, Groupe de recherche et d'édition, (2002).

Kurtosis parameter of superposition of Kummer beams propagating through ABCD optical system

F. Khannous[1], H. Nebdi[1], M. Boustimi[2], A. Belafhal[1] *

[1] Laboratory of Nuclear, Atomic and Molecular Physics
Department of Physics, Faculty of Sciences, Chouaïb Doukkali University,
P. B.: 20, 24000 El Jadida, Morocco

[2] Physics Department, College of Applied Sciences, Umm Al-Qura University,
P.O. Box : 715 , Makkah 21955, Saudi Arabia
* Corresponding authors: belafhal@gmail.com

Abstract

In this study, on the basis of the propagation equation of superposition of Kummer beams and irradiance moments definition, an analytical propagation expression for the kurtosis parameter K of this beams family is derived and illustrated with numerical examples. As a special case, the K parameter of the fundamental Gaussian beam is equal 2 in the polar coordinates. The numerical results shown that the parameter K is affected by the change of the beams order, the topological charge and the beam waist.

1. Introduction

Among the parameters concerning the quality of the beam during its propagation is , which is a useful parameter that allows us to describe different laser beams and predict their quality [1]. This beam propagation factor cannot give further information concerning the shape feature of laser beams, such as the symmetry and degree of flatness (or sharpness). For this reason, we need another parameter called kurtosis parameter K, which is written in terms of the second- and fourth-irradiance moments [2-5]. The kurtosis parameter is used to describe the flatness of laser beams. The irradiance profile of beams is classified as leptokurtic, mesokurtic or platykurtic depending on K being larger, equal or less than 3, which is the kurtosis value of the fundamental Gaussian beam for the one-dimensional case [2]. When the beams propagate through paraxial ABCD optical systems, the K parameter changes with the variation of the axial coordinate along the beams axis z, except for a few beams, such as the fundamental Gaussian and Hermite-Gaussian beams [6]. Recently, researchers have extended the kurtosis parameter for other laser beams various propagating through an ABCD system. The kurtosis of Bessel-modulated Gaussian, Hermite-cosh-Gaussian, Mathieu–Gauss, elegant Hermite-Gaussian and Laguerre Gaussian beams, … have been studied [7-16]. The purpose of this present paper is to investigate the kurtosis parameter of the propagation equation of the superposition of Kummer beams (SKBs). The analytical expression of the kurtosis parameter of SKBs is illustrated by using the propagation formula of SKBs. Some numerical examples are given to illustrate the analytical results.

2. The kurtosis parameter of SKBs

In this section, we determine the propagation expression for the kurtosis parameter of SKBs based on the propagation analytical of SKBs. In the polar coordinate system, the kurtosis parameter of rotationally symmetrical beams can be defined as [1]

$$K = \frac{<r^4>}{<r^2>^2} , \qquad (1)$$

where $<r^2>$ and $<r^4>$ are the second-and fourth-order irradiance moments, which are defined as

$$<r^n> = \frac{1}{p} \int_0^{2\pi} \int_0^{+\infty} r^n \left| E(r,\varphi,z) \right|^2 r dr d\varphi, \qquad n = 2,4. \qquad (2)$$

In this last equation, p is the total power of the beam, and its expression is given by

$$p = \int_0^{2\pi} \int_0^{+\infty} \left| E(r,\varphi,z) \right|^2 r dr d\varphi \ , \qquad (3)$$

and E(r,φ,z) is the field distribution of the SKBs along the z-axis.

Before to determine the kurtosis parameter, first, we should evaluate in our case, the expression of the second- and fourth-order irradiance moments. The propagation equation of SKBs passing through a paraxial ABCD optical system is given by [17]

$$E(r,\varphi,z) = A_0 2\pi \frac{(-i)^{|l|+1}}{\lambda B} \left(\frac{kr}{B} \right)^{|l|} \frac{1}{\Gamma(|l|+1)2^{|l|+1}} \exp[i(l\varphi + k(z))] e^{i\frac{kD}{2B}r^2}$$

$$\times \sum_{n=0}^{N} C_n^{(N)} \sum_{m=0}^{n} \binom{n}{n-m} \frac{(-1)^m \left(\frac{2}{w_N^2(0)} \right)^m}{m!} \frac{\Gamma\left(\frac{|l|}{2} + m + 1 \right)}{\alpha^{\frac{|l|}{2}+m+1}} {}_1F_1\left(\frac{|l|}{2} + m + 1; |l| + 1; -\frac{k^2 r^2}{4\alpha B^2} \right) \qquad ,(4)$$

where $\alpha = \frac{1}{w_N^2(0)} - \frac{ik}{2B} A$, $w_N(0) = \frac{w_0}{\sqrt{N+1}}$, $C_n^{(N)} = (-1)^n \sum_{m=n}^{N} \frac{1}{2^m} \binom{m}{n}$, is a complex factor, l is the

topological charge, is the beam waist and ${}_1F_1$ is the confluent hypergeometric function. Substituting Eq. (3) and Eq. (4) into Eq. (2), one obtains the expression of the second-order irradiance moments

$$<r^2> = \frac{\sum_{n=0}^{N} C_n^{(N)} \sum_{m=0}^{n} \binom{n}{n-m} \frac{(-1)^m \left(\frac{2}{w_N^2(0)} \right)^m}{m!} \sum_{n'=0}^{N} C_{n'}^{(N)} \sum_{m'=0}^{n'} \binom{n'}{n'-m'} \frac{(-1)^{m'} \left(\frac{2}{w_N^2(0)} \right)^{m'}}{m'!} \frac{\Gamma\left(\frac{|l|}{2} + m + 1 \right) \Gamma\left(\frac{|l|}{2} + m' + 1 \right)}{\alpha^{\frac{|l|}{2}+m+1} \alpha^{*\frac{|l|}{2}+m'+1}}}{\sum_{n=0}^{N} C_n^{(N)} \sum_{m=0}^{n} \binom{n}{n-m} \frac{(-1)^m \left(\frac{2}{w_N^2(0)} \right)^m}{m!} \sum_{n'=0}^{N} C_{n'}^{(N)} \sum_{m'=0}^{n'} \binom{n'}{n'-m'} \frac{(-1)^{m'} \left(\frac{2}{w_N^2(0)} \right)^{m'}}{m'!} \frac{\Gamma\left(\frac{|l|}{2} + m + 1 \right) \Gamma\left(\frac{|l|}{2} + m' + 1 \right)}{\alpha^{\frac{|l|}{2}+m+1} \alpha^{*\frac{|l|}{2}+m'+1}}}. \qquad (5)$$

$$\times \frac{\int_0^{+\infty} r^{2|l|+3} {}_1F_1\left(\frac{|l|}{2} + m + 1; |l| + 1; -\frac{k^2 r^2}{4B^2\alpha} \right) {}_1F_1\left(\frac{|l|}{2} + m' + 1; |l| + 1; -\frac{k^2 r^2}{4B^2\alpha^*} \right) dr}{\int_0^{+\infty} r^{2|l|+1} {}_1F_1\left(\frac{|l|}{2} + m + 1; |l| + 1; -\frac{k^2 r^2}{4B^2\alpha} \right) {}_1F_1\left(\frac{|l|}{2} + m' + 1; |l| + 1; -\frac{k^2 r^2}{4B^2\alpha^*} \right) dr}$$

By using the next two formulas [18, 19]

$${}_1F_1(a;b;-z) = e^{-z} {}_1F_1(b-a;b;z), \qquad (6)$$

and

$${}_1F_1(a;b;z) = \sum_{n=0}^{+\infty} \frac{(a)_n}{(b)_n} \frac{z^n}{n!} \ , \qquad (7)$$

the first integral of Eq. (5) can be written as

$$I_1 = \sum_{n=0}^{+\infty} \frac{\left(\frac{|l|}{2} - m\right)_n \left(\frac{k^2}{4B^2\alpha}\right)^n}{(|l|+1)_n} \frac{1}{n!} \int_0^{+\infty} r^{2|l|+3+2n} e^{-\frac{k^2r^2}{4B^2}\left(\frac{1}{\alpha}+\frac{1}{\alpha^*}\right)} {}_1F_1\left(\frac{|l|}{2} - m'; |l|+1; \frac{k^2r^2}{4B^2\alpha^*}\right) dr. \tag{8}$$

Putting x= and making use the integral formula [20]

$$\int_0^\infty x^{\delta-1} \exp(-\mu x) {}_mF_n(\alpha_1, \alpha_2, ..., \alpha_m; \beta_1, \beta_2, ..., \beta_n; \lambda x) dx = \Gamma(\delta)\mu^{-\delta}{}_{m+1}F_n\left(\alpha_1, \alpha_2, ..., \alpha_m; \delta; \beta_1, \beta_2, ..., \beta_n; \frac{\lambda}{\mu}\right), \tag{9}$$

with $m \le n$, $\mathrm{Re}\,\delta > 0$, $\mathrm{Re}\,\mu > 0$, *if* $m < n$; $\mathrm{Re}\,\mu > \lambda$, *if* $m = n$, Eq. (8) becomes

$$I_1 = \frac{1}{2} \sum_{n=0}^{+\infty} \frac{\left(\frac{|l|}{2} - m\right)_n \left(\frac{k^2}{4B^2\alpha}\right)^n}{(|l|+1)_n} \frac{1}{n!} \Gamma(|l|+n+2) \left(\frac{k^2}{4B^2}\left(\frac{1}{\alpha}+\frac{1}{\alpha^*}\right)\right)^{-|l|-n-2} {}_2F_1\left(\frac{|l|}{2} - m', |l|+n+2; |l|+1; \frac{\alpha}{\alpha+\alpha^*}\right). \tag{10}$$

On the other hand, using the equations (6), (7) and (9), the second integral in Eq. (5) is equal to

$$\begin{aligned} I_2 &= \sum_{n=0}^{+\infty} \frac{\left(\frac{|l|}{2} - m\right)_n \left(\frac{k^2}{4B^2\alpha}\right)^n}{(|l|+1)_n} \frac{1}{n!} \int_0^{+\infty} r^{2|l|+2n+1} e^{-\frac{k^2r^2}{4B^2}\left(\frac{1}{\alpha}+\frac{1}{\alpha^*}\right)} {}_1F_1\left(\frac{|l|}{2} - m'; |l|+1; \frac{k^2r^2}{4B^2\alpha^*}\right) dr \\ &= \frac{1}{2} \sum_{n=0}^{+\infty} \frac{\left(\frac{|l|}{2} - m\right)_n \left(\frac{k^2}{4B^2\alpha}\right)^n}{(|l|+1)_n} \frac{1}{n!} \Gamma(|l|+n+1) \left(\frac{k^2}{4B^2}\left(\frac{1}{\alpha}+\frac{1}{\alpha^*}\right)\right)^{-|l|-n-1} {}_2F_1\left(\frac{|l|}{2} - m', |l|+n+1; |l|+1; \frac{\alpha}{\alpha+\alpha^*}\right). \end{aligned} \tag{11}$$

Replacing Eqs. (10) and (11) into Eq. (5), we find

$$<r^2> = \frac{\displaystyle\sum_{n=0}^N C_n^{(N)} \sum_{m=0}^n \binom{n}{n-m} \frac{(-1)^m \left(\frac{2}{w_N^2(0)}\right)^m}{m!} \sum_{n'=0}^N C_{n'}^{(N)} \sum_{m'=0}^{n'} \binom{n'}{n'-m'} \frac{(-1)^{m'} \left(\frac{2}{w_N^2(0)}\right)^{m'}}{m'!} \frac{\Gamma\left(\frac{|l|}{2}+m+1\right)\Gamma\left(\frac{|l|}{2}+m'+1\right)}{\alpha^{\frac{|l|}{2}+m+1}\alpha^{*\frac{|l|}{2}+m'+1}}}{\displaystyle\sum_{n=0}^N C_n^{(N)} \sum_{m=0}^n \binom{n}{n-m} \frac{(-1)^m \left(\frac{2}{w_N^2(0)}\right)^m}{m!} \sum_{n'=0}^N C_{n'}^{(N)} \sum_{m'=0}^{n'} \binom{n'}{n'-m'} \frac{(-1)^{m'} \left(\frac{2}{w_N^2(0)}\right)^{m'}}{m'!} \frac{\Gamma\left(\frac{|l|}{2}+m+1\right)\Gamma\left(\frac{|l|}{2}+m'+1\right)}{\alpha^{\frac{|l|}{2}+m+1}\alpha^{*\frac{|l|}{2}+m'+1}}}$$

$$\times \frac{\displaystyle\sum_{n=0}^{+\infty} \frac{\left(\frac{|l|}{2}-m\right)_n \left(\frac{k^2}{4B^2\alpha}\right)^n}{(|l|+1)_n} \frac{1}{n!} \Gamma(|l|+n+2)\left(\frac{k^2}{4B^2}\left(\frac{1}{\alpha}+\frac{1}{\alpha^*}\right)\right)^{-|l|-n-2} {}_2F_1\left(\frac{|l|}{2}-m', |l|+n+2; |l|+1; \frac{\alpha}{\alpha+\alpha^*}\right)}{\displaystyle\sum_{n=0}^{+\infty} \frac{\left(\frac{|l|}{2}-m\right)_n \left(\frac{k^2}{4B^2\alpha}\right)^n}{(|l|+1)_n} \frac{1}{n!} \Gamma(|l|+n+1)\left(\frac{k^2}{4B^2}\left(\frac{1}{\alpha}+\frac{1}{\alpha^*}\right)\right)^{-|l|-n-1} {}_2F_1\left(\frac{|l|}{2}-m', |l|+n+1; |l|+1; \frac{\alpha}{\alpha+\alpha^*}\right)}. \tag{12}$$

Similar calculations have been performed to determinate the fourth-order irradiance moments. So, we found

$$
<r^4> = \frac{\displaystyle\sum_{n=0}^{N} C_n^{(N)} \sum_{m=0}^{n} \binom{n}{n-m} \frac{(-1)^m \left(\frac{2}{w_N^2(0)}\right)^m}{m!} \sum_{n'=0}^{N} C_{n'}^{(N)} \sum_{m'=0}^{n'} \binom{n'}{n'-m'} \frac{(-1)^{m'} \left(\frac{2}{w_N^2(0)}\right)^{m'}}{m'!} \frac{\Gamma\left(\frac{|l|}{2}+m+1\right)\Gamma\left(\frac{|l|}{2}+m'+1\right)}{\alpha^{\frac{|l|}{2}+m+1} \alpha^{*\frac{|l|}{2}+m'+1}}}{\displaystyle\sum_{n=0}^{N} C_n^{(N)} \sum_{m=0}^{n} \binom{n}{n-m} \frac{(-1)^m \left(\frac{2}{w_N^2(0)}\right)^m}{m!} \sum_{n'=0}^{N} C_{n'}^{(N)} \sum_{m'=0}^{n'} \binom{n'}{n'-m'} \frac{(-1)^{m'} \left(\frac{2}{w_N^2(0)}\right)^{m'}}{m'!} \frac{\Gamma\left(\frac{|l|}{2}+m+1\right)\Gamma\left(\frac{|l|}{2}+m'+1\right)}{\alpha^{\frac{|l|}{2}+m+1} \alpha^{*\frac{|l|}{2}+m'+1}}} \quad (13)
$$

$$
\times \frac{\displaystyle\sum_{n=0}^{+\infty} \frac{\left(\frac{|l|}{2}-m\right)_n \left(\frac{k^2}{4B^2\alpha}\right)^n}{(|l|+1)_n \, n!} \Gamma(|l|+n+3) \left(\frac{k^2}{4B^2}\left(\frac{1}{\alpha}+\frac{1}{\alpha^*}\right)\right)^{-|l|-n-3} {}_2F_1\left(\frac{|l|}{2}-m', |l|+n+3; |l|+1; \frac{\alpha}{\alpha+\alpha^*}\right)}{\displaystyle\sum_{n=0}^{+\infty} \frac{\left(\frac{|l|}{2}-m\right)_n \left(\frac{k^2}{4B^2\alpha}\right)^n}{(|l|+1)_n \, n!} \Gamma(|l|+n+1) \left(\frac{k^2}{4B^2}\left(\frac{1}{\alpha}+\frac{1}{\alpha^*}\right)\right)^{-|l|-n-1} {}_2F_1\left(\frac{|l|}{2}-m', |l|+n+1; |l|+1; \frac{\alpha}{\alpha+\alpha^*}\right)}.
$$

Finally, substituting Eqs. (12) and (13) into Eq. (1), the propagation equation of the kurtosis parameter is obtained as follow

$$
K = \frac{\displaystyle\sum_{n=0}^{N} C_n^{(N)} \sum_{m=0}^{n} \binom{n}{n-m} \frac{(-1)^m \left(\frac{2}{w_N^2(0)}\right)^m}{m!} \sum_{n'=0}^{N} C_{n'}^{(N)} \sum_{m'=0}^{n'} \binom{n'}{n'-m'} \frac{(-1)^{m'} \left(\frac{2}{w_N^2(0)}\right)^{m'}}{m'!} \frac{\Gamma\left(\frac{|l|}{2}+m+1\right)\Gamma\left(\frac{|l|}{2}+m'+1\right)}{\alpha^{\frac{|l|}{2}+m+1} \alpha^{*\frac{|l|}{2}+m'+1}}}{\displaystyle\sum_{n=0}^{N} C_n^{(N)} \sum_{m=0}^{n} \binom{n}{n-m} \frac{(-1)^m \left(\frac{2}{w_N^2(0)}\right)^m}{m!} \sum_{n'=0}^{N} C_{n'}^{(N)} \sum_{m'=0}^{n'} \binom{n'}{n'-m'} \frac{(-1)^{m'} \left(\frac{2}{w_N^2(0)}\right)^{m'}}{m'!} \frac{\Gamma\left(\frac{|l|}{2}+m+1\right)\Gamma\left(\frac{|l|}{2}+m'+1\right)}{\alpha^{\frac{|l|}{2}+m+1} \alpha^{*\frac{|l|}{2}+m'+1}}}
$$

$$
\times \frac{\displaystyle\sum_{n=0}^{+\infty} \frac{\left(\frac{|l|}{2}-m\right)_n \left(\frac{k^2}{4B^2\alpha}\right)^n}{(|l|+1)_n \, n!} \Gamma(|l|+n+3) \left(\frac{k^2}{4B^2}\left(\frac{1}{\alpha}+\frac{1}{\alpha^*}\right)\right)^{-|l|-n-3} {}_2F_1\left(\frac{|l|}{2}-m', |l|+n+3; |l|+1; \frac{\alpha}{\alpha+\alpha^*}\right)}{\displaystyle\sum_{n=0}^{+\infty} \frac{\left(\frac{|l|}{2}-m\right)_n \left(\frac{k^2}{4B^2\alpha}\right)^n}{(|l|+1)_n \, n!} \Gamma(|l|+n+1) \left(\frac{k^2}{4B^2}\left(\frac{1}{\alpha}+\frac{1}{\alpha^*}\right)\right)^{-|l|-n-1} {}_2F_1\left(\frac{|l|}{2}-m', |l|+n+1; |l|+1; \frac{\alpha}{\alpha+\alpha^*}\right)}
$$

$$
\times \left[\frac{\displaystyle\sum_{n=0}^{N} C_n^{(N)} \sum_{m=0}^{n} \binom{n}{n-m} \frac{(-1)^m \left(\frac{2}{w_N^2(0)}\right)^m}{m!} \sum_{n'=0}^{N} C_{n'}^{(N)} \sum_{m'=0}^{n'} \binom{n'}{n'-m'} \frac{(-1)^{m'} \left(\frac{2}{w_N^2(0)}\right)^{m'}}{m'!} \frac{\Gamma\left(\frac{|l|}{2}+m+1\right)\Gamma\left(\frac{|l|}{2}+m'+1\right)}{\alpha^{\frac{|l|}{2}+m+1} \alpha^{*\frac{|l|}{2}+m'+1}}}{\displaystyle\sum_{n=0}^{N} C_n^{(N)} \sum_{m=0}^{n} \binom{n}{n-m} \frac{(-1)^m \left(\frac{2}{w_N^2(0)}\right)^m}{m!} \sum_{n'=0}^{N} C_{n'}^{(N)} \sum_{m'=0}^{n'} \binom{n'}{n'-m'} \frac{(-1)^{m'} \left(\frac{2}{w_N^2(0)}\right)^{m'}}{m'!} \frac{\Gamma\left(\frac{|l|}{2}+m+1\right)\Gamma\left(\frac{|l|}{2}+m'+1\right)}{\alpha^{\frac{|l|}{2}+m+1} \alpha^{*\frac{|l|}{2}+m'+1}}} \right.
$$

$$
\left. \times \frac{\displaystyle\sum_{n=0}^{+\infty} \frac{\left(\frac{|l|}{2}-m\right)_n \left(\frac{k^2}{4B^2\alpha}\right)^n}{(|l|+1)_n \, n!} \Gamma(|l|+n+2) \left(\frac{k^2}{4B^2}\left(\frac{1}{\alpha}+\frac{1}{\alpha^*}\right)\right)^{-|l|-n-2} {}_2F_1\left(\frac{|l|}{2}-m', |l|+n+2; |l|+1; \frac{\alpha}{\alpha+\alpha^*}\right)}{\displaystyle\sum_{n=0}^{+\infty} \frac{\left(\frac{|l|}{2}-m\right)_n \left(\frac{k^2}{4B^2\alpha}\right)^n}{(|l|+1)_n \, n!} \Gamma(|l|+n+1) \left(\frac{k^2}{4B^2}\left(\frac{1}{\alpha}+\frac{1}{\alpha^*}\right)\right)^{-|l|-n-1} {}_2F_1\left(\frac{|l|}{2}-m', |l|+n+1; |l|+1; \frac{\alpha}{\alpha+\alpha^*}\right)} \right]^{-2}, \quad (14)
$$

where $_2F_1$ is the hypergeometric function. This last equation represents the analytical expression of the kurtosis parameter of the SKBs. This equation indicates that the kurtosis parameter of this family beams depends on the variation of the beam order, the topological charge and the beam waist. For the case of N=l=0, Eq. (14) reduces to K=2, which is the kurtosis parameter of the fundamental Gaussian beam [8, 16].

To analyze the effect of the above parameters to the evolution of the kurtosis one, some numerical calculations were performed using Eq. (14). We assume that the ABCD optical system is a free space with the matrix elements A=1, B=z, C=0, D=1. Plots in Fig .1   to the evolution of kurtosis parameter K of SKBs propagating through ABCD optical system for different propagation distances written in terms of the equivalent Fresnel number F=/λz, and for two values of the topological charge l=1 and l=3, with different values of N.

(a)   **(b)**
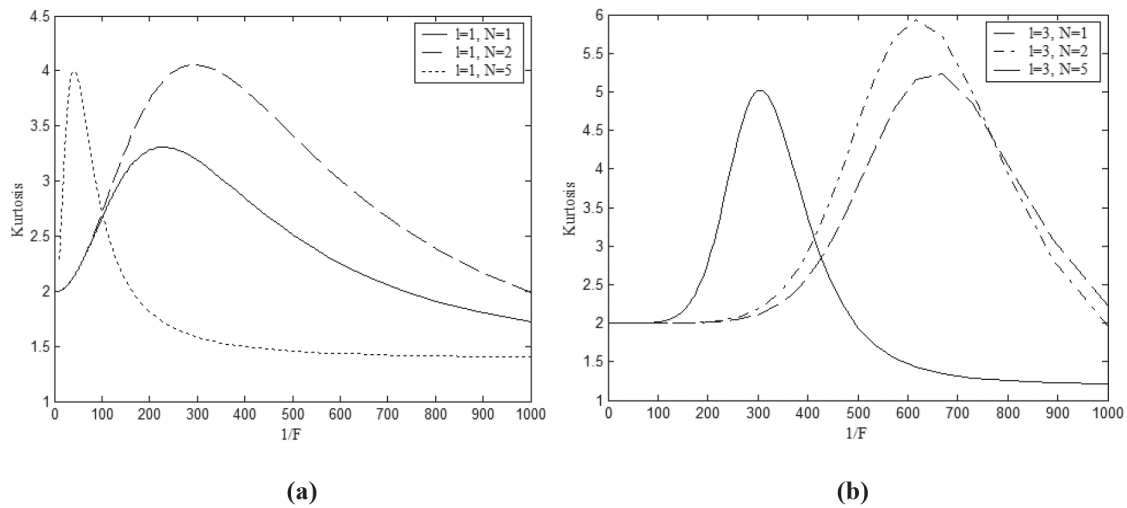
Figure 1: Evolution of kurtosis parameter K of SKBs as function of the inverse of the Fresnel number F for two values of the topological charge (a) l=1, (b) l=3, with several different values of N. The other parameters are =2 mm and λ=1.55μm.

It is clearly seen from this figure that the change of N makes moving the position of the maximum of kurtosis parameter of SKBs, such as the increasing of N, produces a decreasing of this maximum. Also, one finds from Fig. 1, with the increasing of the topological charge, the maximum of kurtosis of SKBs moves and decreases with the increase of propagation distance.

Fig. 2 shows the effect of the beam waist on kurtosis parameter of SKBs in different propagation distances. From this figure, we can observe that, with the increasing of the beam waist, the kurtosis of SKBs have a moving *maximum* and decreases with the increasing of propagation distance. This means that the   profile becomes sharper as   increased.
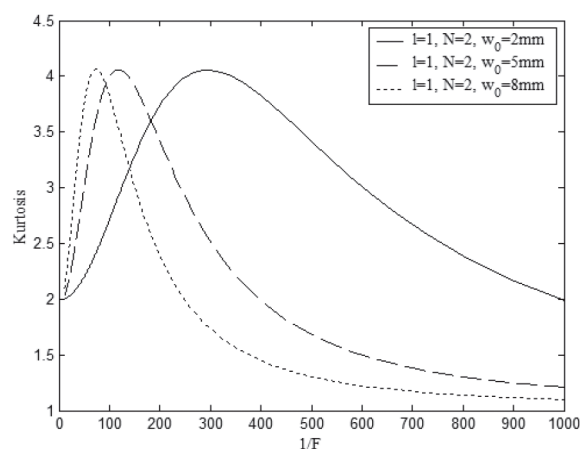
Figure 2: Evolution of kurtosis parameter K of SKBs as function of the inverse of the Fresnel number F for different values of . The other parameters are l=1, N=2, and λ=1.55μm.

3. Conclusion

In this work, the analytical expression for the kurtosis parameter of SKBs is derived on the basis of the propagation equation of the SKBs propagating through a paraxial ABCD optical system. The obtained results showed that, the kurtosis parameter of SKBs changes with the variation of the beam order, the topological charge and the beam waist . In addition, the K parameter of the fundamental Gaussian is obtained as a special case and illustrated.

References

[1] A. E. Siegman, Optical Resonators, 1224 (1990) 2-14.

[2] P. M. Mejias, H. Weber, R. Martinez-Herrero, A. Gonzalez-Urena (eds.), Proceeding of Laser Beam Characterization, Seceded Espanda Optica, Madrid, Spain, (1993).

[3] R. Martinez-Herrero, G. Piquero, P. M. Mejias, Opt. Commun., 115(1 995) 225-232.

[4] H. Weber, Opt. Quantum Electron., 24 (1992) 1027–1049

[5] R. Martinez-Herrero, P. M. Mejias, M. Sanchez, J. L. H Neira, Opt. Quantum Electron., 24 (1992) 1021–1026.

[6] R. Martinez-Herrero, P. M. Mejias, Opt. Lett., 18 (1993) 1669-1671.

[7] S. A. Amarande, Opt. Commun., 129 (1996) 311-317.

[8] A. Chafiq, Z. Hricha, A. Belafhal, Opt. Commun., 282 (2009) 2590–2594.

[9] Z. Hricha, L. Dalil-Essakali, M. Ibnchaikh, A. Belafhal, Phys. Chem. News, 3 (2001) 11-16.

[10] Z. Mei, D. Zhao, Optics & Laser Technology, 39 (2007) 586–592.

[11] S. Luo, B. Lu, Optik, 113 (2002) 329–332.

[12] S. Luo, B. Lu, Optik, 113 (2002) 227–231.

[13] H. Mao, D. Zhao, Optik, 118 (2007) 57–61.

[14] G. Zhou, Optics & Laser Technology, 41 (2009) 953–955.

[15] Z. Mei, D. Zha, D. Sun, J. Gu, Optik, 115 (2004) 89–93.

[16] B. Lu, X. Wang, Opt. Commun., 204 (2002) 91–97.

[17] F. Khannous, L. Ez-zariy, H. Nebdi, M. Khouilid, A. Belafhal, Phys. Chem. News, 70 (2013) 41-49.

[18] M. Abramowitz, I. A. Stegun (eds.), Handbook of Mathematical Functions with Formulas, Graphs, and Mathematical Tables, National Bureau of Standards, Washington, DC, (1964).

[19] H. Buchholz, The Confluent Hypergeometric Function with Special Emphasis on its Applications, Springer, New York, (1969).

[20] I. S. Gradshteyn, I. M. Ryzhik, Tables of Integrals, Series and Products, 5th ed., Academic Press, New York, (1994).

Instructions for authors

1. Type of Manuscripts
2. Organization of the Manuscript
3. Language
4. Submission of the Manuscript
5. Peer Review
6. Revision of the Manuscript
7. Special Features, Appendices and Supplementary Material
8. Preprint Option
9. Publication of the Manuscript

Frontiers in Science and Engineering an International Journal edited by Hassan II Academy of Science and Technology uses author-supplied PDFs for all online and print publication.

1. Type of Manuscripts
The FSE Journal publishes the following article types :
Reviews/State of the art, usually through Academy invitation and organized into themed issues, report on recent advances in science and technology. 20 pages maximum according to the format given.
Original Research Papers contain innovative and hypothesis-driven research; supported by sound experimental design, methodology, proofs, and data interpretation. 16 pages maximum according to the format given.
Letters to the Editor: May be submitted by readers commenting articles already published by the Journal. 1 to 2 pages maximum according to the format given.

2. Organization of the Manuscript
The entire manuscript, including mathematical equations, flow-sheets, chemical structures, tables, and figures must be prepared in electronic form and submitted as pdf files. Use Times New Roman size 12. For all special characters (e.g., Greek characters) use the font Symbol. Use carriage returns only to end headings and paragraphs, not to break lines of text. Automatic hyphenation should be turned off. Do not insert spaces before punctuation. Verify the correct spelling for the final version with the Spelling and Grammar function of Word.

3. Language
Manuscripts should be written in English.

4. Submission of the Manuscript
The manuscript and supplementary material must be send by the corresponding author to the Editor in an electronic form as pdf files.
You may be required to register as a new user within the Publication System Manager upon your first visit. Straightforward login and registration procedures can be found on the website. Editorial Manager allows authors to track the progress of manuscript review in real time. Detailed, step-by-step instructions for submitting manuscripts can be found on the website. All correspondence regarding your manuscript must go through Publication System Manager.
Authors are asked to prepare their papers, and PDF files, according to the templates and guidelines provided below.

The author(s) need to supply the following items :
• the PDF file of the paper
• a signed Assignment of Copyright Form (once the paper accepted)

We highly recommend that authors prepare their papers/PDFs using the following Microsoft Word or LaTeX templates, which can be downloaded from the following links :
• Microsoft guidelines and templates
• Latex guidelines and class file

A copyright license form will be provided to the corresponding author only when a paper is accepted for publication.

5. Peer Review
All submissions will be reviewed anonymously by at least two independent referees, and a referee should never communicate directly with an author. A referee must treat as confidential material the manuscript and any supplementary material. Authors may suggest names and email addresses of expert reviewers, but selection remains a prerogative of the Editors. Authors may include supplementary notes to facilitate the review process. If an accepted paper is cited

that has not yet appeared in print and is required for evaluation of the submitted manuscript, authors should provide an electronic version for use by the Reviewers. Authors are responsible for all statements in their work, including changes made by the copy editor after a manuscript is accepted.

6. Revision of the Manuscript

All comments made by referees must be addressed. A letter describing all changes that were made should be attached with the revised version of the manuscript. A copyright license form must accompany the final version of the manuscript.

7. Special Features, Appendices and Supplementary Material

Special features containing highly interactive features or large databases can be included. All authors are encouraged to take advantage WEB online publishing capabilities (i.e. 3-D, video, and interactive graphics). All special features must be created by the Author›s).

Authors who wish to publish electronic supplementary material to their article (Excel files, images, audio/video files) must submit the supplementary files/materials with their manuscript submission via our online peer review tracking Publication System Manager. Note that supplementary files are not automatically included in the reviewer PDF. Please therefore note in the cover letter if these materials should be evaluated by reviewers.

8. Preprint Option

Before making a PDF file of your article, please check the following tips in the next section.

Article checklist

There are a number of essential basic requirements which must be followed during preparation of your article. If article PDFs are prepared without following these essential requirements, publication may be delayed until a usable and compatible PDF is received.

Articles must not contain page numbers, headers or footers

This is extremely important. Page numbers, copyright details etc are added by the Publication System Manager Publishing during the production and publication process. If you put page numbers on your paper we will have to contact you for a replacement PDF, which could delay publication.

Article margins must be adequate

We recommend a minimum 15mm all round. The Microsoft Word template or Latex templates automatically provide the correct margins so their use is highly recommended.

All articles must have an abstract

When readers are searching for information online, an abstract of an article is the first thing they see. Your abstract needs to be concise but convey as much information as possible about the content of your article. In addition, our Publication System Manager Publishing will supply your abstract to many other database systems used by researchers to find papers.

Addresses should be complete and include the country and a contact name

The title of the article, author names with full first name (no degrees), each author's affiliation, and a suggested running head (of less than 50 characters, including spaces). The affiliation should comprise the department, institution (usually university or company), city, and country and should be typed as a footnote to the author's name. For the corresponding author designated to correspond with the Editorial Office and review proofs, indicate his/her complete mailing address, office/cellular telephone number, fax number, and e-mail address. During production of the electronic paper we may need to contact you if there is something to check or for a request a replacement PDF file.

References should be complete and carefully formatted

Online versions of all reference lists will, wherever possible, be electronically linked to the articles that you cite. Reference lists containing many links direct to the cited paper are a valuable research tool. The time and effort spent in preparing your references, so that they can be linked, will be very appreciated by readers of your paper. Please, notice also that all the citations should be justified according to the contents of the proposed article. Abusive citations of the same author may induce a certain delay in the overall review process

PrePrint

Any manuscript received for publication in FSE can be published on the Web as preprint. All authors submitting a manuscript must clearly indicate that they wish to publish it as a preprint. The referees appreciate if the manuscript meets the basic requirements for publication and recommend its publication as preprint. A preprint not accepted for publication by the referees will be immediately removed from the preprint collection. A published paper which was previously available as a preprint will have clearly indicated the date when it was first published on the Web. A work published as preprint can benefit from comments from the readers which can eventually improve the manuscript. Revised versions that incorporate corrections from reviewers and suggestions from readers can be also published as preprints.

9. Publication of the Manuscript

Accepted papers are published as PDF files available at the Web site of the Academy.

Transfer of Copyright Form

A signed copy of the Transfer of Copyright must be submitted online as part of the manuscript submission process (FSECopyright.pdf).

Astract

Reviews/State of the Art, Original Research Articles, require an abstract. The abstract is limited to 300 words or less. For Research Articles, the abstract should include a brief statement for each of the sections related to Introduction, Methods/Approaches/Materials and Discussion, and Conclusion written in paragraph form. All abstracts must be written in one paragraph, with no subheadings, equations, tables, reference citations or graphics.

Keywords

Provide a list of no more than 5 key words.

Introduction

Required for Reviews/State of the art and Original Research Articles.

Main Text Body

For Original Research Articles, organize the main text as follows: Introduction, Approach/Materials and Methods, Results, Discussion, and Conclusion. The use of subheadings to divide the text is encouraged. Primary, Secondary, and Third level headings should be clearly defined, but do not use numbers or letters.

Recommended word counts are as follows: Reviews/State of the art: 8000, Original Research Articles : 6000.

Use abbreviations sparingly, and define them at the first insertion in the text. Use the metric system for all measurements. Express metric abbreviations in lowercase letters without periods (cm, ml, sec). Define all symbols used in equations and formulas. When symbols are used extensively, the authors may include a list of all symbols in a table.

Conclusion

The conclusion should be a brief paragraph, containing 3 to 4 sentences, that summarizes the findings presented.

Acknowledgments

Include funding source(s) and other contributions. If the work has been funded by any organisation please provide name(s) of funding institute(s) and grant number(s).

References

References should conform to Vancouver style and be numbered consecutively in the order in which they are cited in the text. Cite in the text by the appropriate Arabic numeral enclosed in parentheses, e.g., (1), (2-5), etc.

It is advisable to limit the maximum number of references as really needed only.

References to unpublished peer-reviewed, personal communications, including conference abstracts, and papers in preparation or in review, cannot be listed, but can be notated parenthetically in the text.

Abbreviations for journal names should conform to those of Vancouver style (as depicted in http://www.library. uq.edu.au/training/citation/vancouv.pdf). The style and punctuation of the references should conform to conventional referencing.

Whenever, the paper is not yet published officially but accepted, please write down the corresponding DOI within the reference.

Authors may identify uniform resource locators (URLs) for websites that provide the reader with additional information on the topic addressed in the manuscript. Although URLs are an important feature of electronic publishing, authors are encouraged to be very selective in their choice of sites to include. Do not include links to sites that are not accessible without a password.

All on-line documents should contain author(s), title, On-line document/ Web /FTP /organisation /On-line database/ Supplementary material/ Private homepage , and Accessed Day Month Year, so that readers can refer to.

Tables

Tables must be created in Microsoft Word /Latex table format. Tables should be numbered (with Roman numerals) and referred to by number in the text. Center the title above the table, and type explanatory footnotes (indicated by superscript lowercase letters) below the table. Data must be placed in separate cells of the table to prevent text and numbers from shifting when the table is converted for publication on the Internet. Empty cells may be inserted to create spacing. Tables should not duplicate information provided in the text. Instead, tables should be used to provide additional information that illustrates or expands on a specific point the author wishes to make. Each table should be self-explanatory.

Figures

The FSE offers authors the use of color figures in online published manuscripts. Figures (as well as photographs, drawings, diagrams, and charts) are to be numbered in one consecutive series of Arabic numerals in the order in which they are cited in the text. All Electronic artwork must be submitted online via our online peer review tracking system, Publication System Manager.

The maximum combined count for tables and figures for papers should not exceed 15 to 20.

Footnotes

Footnotes should be avoided. When their use is absolutely necessary, footnotes should be numbered consecutively using Arabic numerals and should be typed at the bottom of the page to which they refer. Place a line above the footnote, so that it is set off from the text. Use the appropriate superscript numeral for citation in the text.

Guidelines

We highly recommend that authors prepare their papers/PDFs using the following Microsoft Word or LaTeX templates, which can be downloaded from the following links:

• Latex guidelines and class file http://www.academie.hassan2.sciences.ma/fse/FSE%20Sample%20cls.tex.txt

• PDF guidelines and templates http://www.academie.hassan2.sciences.ma/fse/FSE%20Sample%20cls.pdf

• Microsoft word guidelines and templates

Contractual issues

1. Full Disclosure

During the manuscript submission process, all authors will be required to confirm that the manuscript has not been previously published in any language anywhere and that it is not under simultaneous consideration by another journal.

2. Conflicts of Interest

Authors must declare all conflicts of interest (or their absence) in their cover letter upon submission of a manuscript. This conflict declaration includes conflicts or potential conflicts of all listed authors. If any conflicts are declared, FSE publish them with the paper. In cases of doubt, the circumstance should be disclosed so that the editors may assess its significance.

Conflicts may be financial, academic, commercial, political or personal. Financial interests may include employment, research funding (received or pending), stock or share ownership, patents, payment for lectures or travel, consultancies, nonfinancial support, or any fiduciary interest in a company.

3. Copyright Transfer

The Copyright Revision Act requires that Authors transfer their copyrights to the Publisher, HIIAST, in order to provide for the widest possible dissemination of professional and scientific literature. A signed Transfer of Copyright form must be submitted online with the manuscript. The Transfer of Copyright form for an accepted manuscript must be on file with the HIIAST Editorial Office prior to production for publication. Corresponding Authors may print and sign the form on behalf of all authors The Transfer of Copyright form can be found at fsecopyright.pdf.

4. Use of Copyrighted Tables and Figures

A copy of the granted permission to use copyrighted figures and tables must be included with the submitted manuscript.

ACADEMY Press MA